A mathematical model of fluid flow in a scraped surface heat exchanger

B. R. Duffy, S. K. Wilson
Department of Mathematics, University of Strathclyde, Livingstone Tower, 26 Richmond Street, Glasgow G1 1XH, UK. Email: b.r.duffy@strath.ac.uk, s.k.wilson@strath.ac.uk

M. E. M. Lee
BP Institute for Multiphase Flow, Bullard Laboratories, Madingley Road, Cambridge CB3 0EZ, UK. Email: michael@bpi.cam.ac.uk

15th July 2005, revised 29th August 2006

Abstract. A simple mathematical model of fluid flow in a common type of scraped surface heat exchanger in which the gaps between the blades and the device walls are narrow, so that a lubrication-theory description of the flow is valid, is presented. Specifically steady isothermal flow of a Newtonian fluid around a periodic array of pivoted scraper blades in a channel with one stationary and one moving wall, when there is an applied pressure gradient in a direction perpendicular to the wall motion, is analysed. The flow is three-dimensional, but decomposes naturally into a two-dimensional "transverse" flow driven by the boundary motion and a "longitudinal" pressure-driven flow. Firstly details of the structure of the transverse flow are derived, and, in particular, the equilibrium positions of the blades are calculated. It is shown that the desired contact between blades and the moving wall will be attained provided that the blades are pivoted sufficiently close to their ends. When the desired contact is achieved the model predicts that the forces and torques on the blades are singular, and so the model is generalised to include three additional physical effects, namely non-Newtonian power-law behaviour, slip at rigid boundaries, and cavitation in regions of very low pressure, each of which is shown to resolve these singularities. Lastly the nature of the longitudinal flow is discussed.

Keywords: lubrication theory, scraped surface heat exchanger

1. Introduction

Scraped surface heat exchangers (SSHEs) are widely used in the food industry to cook, chill, crystallize or sterilize certain foodstuffs quickly and efficiently without causing unwanted changes to the constitution, texture and appearance of the final product. A SSHE is essentially a cylindrical steel annulus whose outer wall is heated or cooled externally; the foodstuff is driven slowly by an axial pressure gradient along the annulus, and a "bank" of blades rotating with the inner wall (the "rotor") is used to scrape it away from the outer wall (the "stator"), preventing fouling, and maintaining mixing and heat transfer. In the

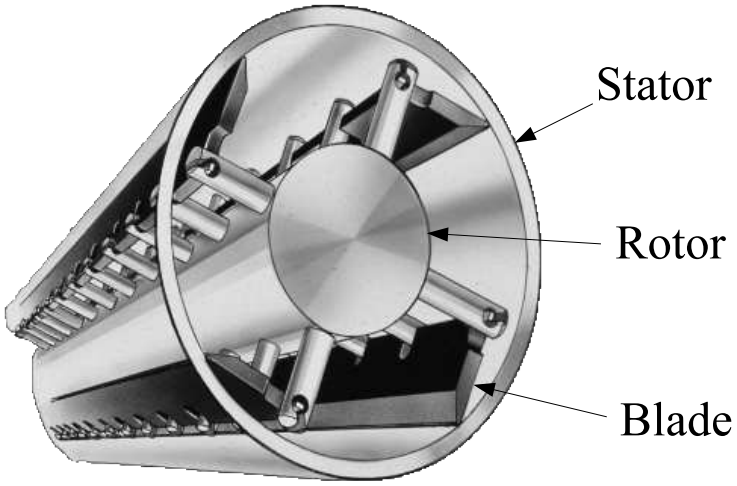

Figure 1. Cutaway sketch of a four-bladed scraped surface heat exchanger (SSHE). (Based on a figure provided to us by Tetra Pak and reproduced here with permission.)

mixing process the transverse flow is more significant than the axial flow. The blades typically are arranged in groups of two (180° apart) or four (90° apart); sometimes pairs of blades are "staggered" axially. Figure 1 shows a "cutaway" sketch of a four-bladed SSHE (albeit with a somewhat wider gap between the rotor and stator than the type for which the present mathematical model is valid) which illustrates the general geometry of the device. Sometimes the blades are manufactured with holes in them; the holes allow mass flow through the blades, reducing the power required for rotation.

There are several types of SSHE in use; we shall be concerned with the type that is used for very viscous foodstuffs such as purées, sauces, margarines, jams, spreads, soups, baby-foods, chocolate, mayonnaise, caramel, fudge, ice-cream, cream and yoghurt. In this common type of SSHE the gaps between the blades and both the stator and the rotor are slender, as are the gaps between the stator and the rotor away from the blades.

Foodstuffs commonly behave as non-Newtonian materials, typically being shear-thinning, viscoplastic and/or viscoelastic, as well as being inhomogeneous, and possibly undergoing phase changes; also they often have a strongly temperature-dependent viscosity. Moreover, both

convection and dissipation of heat can be significant in a SSHE. These factors, coupled with the fact that the geometry is complicated, mean that the processes that take place inside SSHEs are complex: operating conditions vary with context, and operators are guided largely by experience and correlations. Thus despite their widespread use, understanding of the behaviour of the material inside SSHEs is still incomplete; features of the behaviour have been analysed recently by, for example, Stranzinger, Feigl and Windhab [1], Fitt and Please [2] and Sun *et al.* [3], and experimental work on SSHEs has been done by, for example, Härröd [4], Wang, Walton and McCarthy [5] and Rodruiguez [6]. Extensive literature surveys are given by Härröd [7, 4], Rodruiguez [6], and Rao and Hartel [8].

The present work forms part of a larger research project on scraped surface heat exchangers involving an interdisciplinary team of academics and industrialists (see [9] for a brief general overview of the project). Specifically, in this paper we present a simple mathematical model of the fluid flow in a SSHE. Since the various gaps in a SSHE of the type considered are slender (the aspect ratios being of order 10^{-1} and the appropriate reduced Reynolds number being of order 10^{-2}) the "lubrication approximation" may be used to analyse the flow (see Fitt and Please [2] and Fitt, Lee and Please [10] for details). Neglect of inertia means that a Galilean shift may be performed on the system, so that the blade and upper wall (rotor) are brought to rest, and it is the lower wall (stator) that moves. Thus we consider steady flow of a viscous fluid around a freely pivoted scraper blade in a periodic array of blades inside a channel with one stationary wall and one moving wall, when there is an applied pressure gradient in a direction perpendicular to the wall motion. The flow is fully three-dimensional, but decomposes naturally into a two-dimensional "transverse" flow driven by the boundary motion and a "longitudinal" pressure-driven flow; for simplicity of presentation these two ingredients are examined separately. In section 2 we suppose that the blade does not make contact with a wall of the channel, whereas in section 3 we suppose that it does. Finally in section 4 the nature of the longitudinal flow is discussed.

Despite the fact that non-Newtonian flow effects can be significant in a real SSHE, in this study we largely restrict attention to the case of a Newtonian fluid; moreover we are concerned only with the fluid flow in the channel, not the heat transfer, and so we consider only isothermal flow. However, even with these simplifications, the simple model presented herein contributes useful insight into the flow inside a SSHE and provides a basis for subsequent studies of more complicated physical effects. For example, in a companion paper Fitt, Lee and Please [10] use the approach of Fitt and Please [2] and the present work to

consider heat flow in a SSHE and, in particular, the possibility of "channelling", the practically very undesirable situation in which material passes through the device without experiencing significant heating or cooling.

An approach of the type used in the present paper may also be useful in analysing other "confined" flows with a narrow geometry involving a pivoted blade or flap that is in contact or near contact with a bounding wall; examples include flap actuators in micro-electro-mechanical systems (Ho and Tai [11], Kaajakari and Lal [12]), prosthetic heart valves (Peskin [13]), agitators and screw extruders, with, for example, spiral impellers and/or baffles (Penney [14]), and hairs inside the cochlea or semi-circular canal of the ear.

2. Two-dimensional flow in a channel with a periodic array of blades

2.1. Formulation

First we consider steady two-dimensional (transverse) flow of an isothermal incompressible Newtonian fluid of viscosity μ in a long parallel-sided channel of width H in which there is a periodic array of inclined smoothly pivoted thin plane blades, the flow being driven by the motion of one wall of the channel parallel to itself with speed U (> 0), the other wall being fixed. In practice, SSHEs are often mounted vertically, and so we shall ignore the effect of gravity on the transverse flow.

We introduce Cartesian axes $Oxyz$ as shown in Figure 2, with the wall $y = 0$ moving with velocity $U\mathbf{i}$, and the wall $y = H$ fixed. Suppose a thin plane freely pivoted blade occupies $0 \leq x \leq L$, with its pivot fixed at $(x_{\rm p}, h_{\rm p})$, where $0 \leq x_{\rm p} \leq L$ and $0 < h_{\rm p} < H \ll L$, and suppose that the separation between the blades is ℓ (≥ 0), so that the portion $L \leq x \leq L + \ell$ of the channel contains no blades. This configuration is repeated periodically, with period $L + \ell$; in the following we shall refer the description to the interval $0 \leq x \leq L + \ell$. In terms of the SSHE, the width H, period $L + \ell$ and speed U are defined by $H = R_2 - R_1$, $L + \ell = 2\pi R_1/N$ and $U = R_1\omega$, where R_1 and R_2 are the radii of the rotor and stator, N is the number of blades in a cross section of the SSHE, and ω is the angular speed of the rotor. The limit $\ell/L \to \infty$ corresponds to the case of a single blade in a channel (and the limit $H/h_{\rm p} \to \infty$ of this case corresponds to the "rocker bearing" in classical lubrication theory, studied extensively by, for example, Raimondi and Boyd [15, 16]).

Let α (which may be positive or negative) denote the angle of inclination of the blade to the x axis, as shown in Figure 2. In the

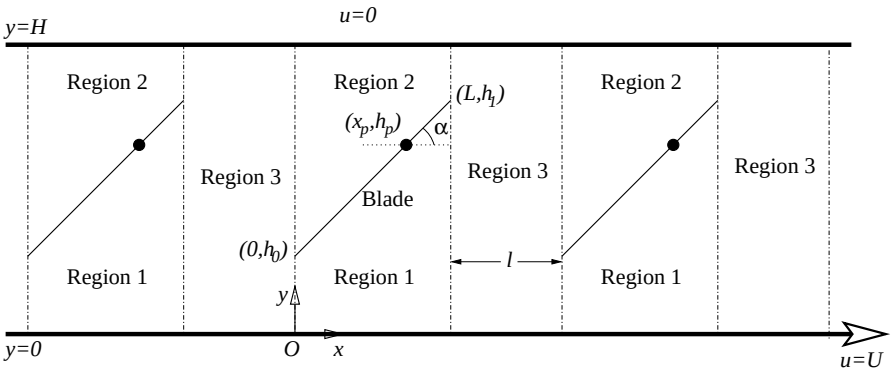

Figure 2. Geometry of the model problem treated in this paper, namely a periodic array of scraper blades in a channel with one stationary wall and one moving wall. The dots signify the positions of the blade pivots.

lubrication-theory approach used here we will assume that $|\alpha| \ll 1$; then the blade is given by $y = h(x)$ for $0 \le x \le L$, where

$$h(x) = h_{\rm p} + \alpha(x - x_{\rm p}). \tag{1}$$

Also we let $h_0 = h(0)$ and $h_1 = h(L)$, so that

$$h_0 = h_{\rm p} - \alpha x_{\rm p}, \quad h_1 = h_{\rm p} + \alpha(L - x_{\rm p}), \quad \alpha = \frac{h_1 - h_0}{L}. \tag{2}$$

For steady flow the blade is in equilibrium, subject to forces due to the fluid, the pivot, and (in general) the walls $y = 0$ and $y = H$ of the channel.

In this section we consider the case when the ends of the blade are *not* in contact with the walls of the channel, so that $0 < h_0, h_1 < H$. The alternative situation in which one of the ends of the blade makes contact with a wall of the channel will be considered in section 3.

We denote the velocities, pressures, volume fluxes (per unit length in the axial direction) and stream functions by $u_k\,\mathbf{i} + v_k\,\mathbf{j}$, p_k, Q_k and ψ_k, where $k = 1$ denotes values in $0 \le x \le L$, $0 \le y \le h$ (that is, the region "below" the blade, termed "region 1"), $k = 2$ denotes values in $0 \le x \le L$, $h \le y \le H$ (that is, the region "above" the blade, termed "region 2"), and $k = 3$ denotes values in $L \le x \le L + \ell$, $0 \le y \le H$

(termed "region 3"). The lubrication approximation[1] gives

$$\mu\frac{\partial^2 u_k}{\partial y^2} = \frac{\partial p_k}{\partial x}, \quad \frac{\partial p_k}{\partial y} = 0, \quad \frac{\partial u_k}{\partial x} + \frac{\partial v_k}{\partial y} = 0 \tag{3}$$

for $k = 1, 2, 3$, to be solved subject to the no-slip conditions

$$\begin{aligned} &u_1 = U \quad \text{on} \quad y = 0, \quad u_1 = 0 \quad \text{on} \quad y = h^-, \\ &u_2 = 0 \quad \text{on} \quad y = h^+, \quad u_2 = 0 \quad \text{on} \quad y = H \end{aligned} \tag{4}$$

in $0 \le x \le L$, and

$$u_3 = U \quad \text{on} \quad y = 0, \quad u_3 = 0 \quad \text{on} \quad y = H \tag{5}$$

in $L \le x \le L + \ell$.

2.2. Non-dimensionalisation

Before proceeding further it is convenient to non-dimensionalise the problem. Several (equally sensible) choices of non-dimensionalisation are available; we choose

$$\begin{aligned} &x = Lx^*, \quad y = h_{\rm p}y^*, \quad x_{\rm p} = Lx_{\rm p}^*, \quad \ell = L\ell^*, \quad \alpha = \frac{h_{\rm p}}{L}\alpha^*, \\ &h = h_{\rm p}h^*, \quad H = h_{\rm p}H^*, \quad h_0 = h_{\rm p}h_0^*, \quad h_1 = h_{\rm p}h_1^*, \\ &u_k = Uu_k^*, \quad p_k = \frac{\mu UL}{h_{\rm p}^2}p_k^*, \quad Q_k = Uh_{\rm p}Q_k^*, \quad \psi_k = Uh_{\rm p}\psi_k^* \end{aligned} \tag{6}$$

for $k = 1$, 2, 3, and immediately drop the superscript stars for convenience. Henceforth all quantities will be non-dimensional unless it is stated otherwise. In particular, the blade now occupies $0 \le x \le 1$, and (1) becomes

$$h = 1 + \alpha(x - x_{\rm p}), \tag{7}$$

where from (2)

$$h_0 = 1 - \alpha x_{\rm p}, \quad h_1 = 1 + \alpha(1 - x_{\rm p}), \quad \alpha = h_1 - h_0, \tag{8}$$

where $0 \le x_{\rm p} \le 1$, $0 < h_0, h_1 < H$ and $H > 1$.

[1] We shall neglect the small $O(H/L)$ regions of non-uniformity at the ends of the blades where the lubrication equations (3) are invalid; thus our solutions will, in general, be discontinuous at $x = 0$ and $x = L$, just as the corresponding classical solutions for lubrication flow in a step bearing are discontinuous at the step. The (small) corrections associated with these non-uniformities could, in principle, be determined if desired.

2.3. Solution for the flow

Solving (3) for u_k for $k = 1, 2, 3$ subject to (4) and (5) yields

$$u_1 = -\frac{p_{1x}}{2}y(h-y) + 1 - \frac{y}{h}, \tag{9}$$

$$u_2 = -\frac{p_{2x}}{2}(H-y)(y-h), \tag{10}$$

$$u_3 = -\frac{p_{3x}}{2}y(H-y) + 1 - \frac{y}{H}, \tag{11}$$

and hence the volume fluxes (per unit length in the axial direction) in the three regions are given by

$$Q_1 = \int_0^h u_1 \,\mathrm{d}y = -\frac{h^3 p_{1x}}{12} + \frac{h}{2}, \tag{12}$$

$$Q_2 = \int_h^H u_2 \,\mathrm{d}y = -\frac{(H-h)^3 p_{2x}}{12}, \tag{13}$$

$$Q_3 = \int_0^H u_3 \,\mathrm{d}y = -\frac{H^3 p_{3x}}{12} + \frac{H}{2}, \tag{14}$$

each of which is a constant (unknown as yet). Therefore

$$p_{1x} = \frac{6}{h^2} - \frac{12Q_1}{h^3}, \quad p_{2x} = -\frac{12Q_2}{(H-h)^3}, \quad p_{3x} = \frac{6}{H^2} - \frac{12Q_3}{H^3} \tag{15}$$

(and we note that p_{3x} is a constant, but that p_{1x} and p_{2x} vary with x, in general). From (9)–(11) and (15) we have

$$u_1 = \frac{[6Q_1 y + h(h-3y)](h-y)}{h^3}, \tag{16}$$

$$u_2 = \frac{6Q_2(H-y)(y-h)}{(H-h)^3}, \tag{17}$$

$$u_3 = \frac{[6Q_3 y + H(H-3y)](H-y)}{H^3}, \tag{18}$$

and the stream functions ψ_k for $k = 1, 2, 3$, satisfying

$$\frac{\partial \psi_1}{\partial y} = u_1, \quad \frac{\partial \psi_2}{\partial y} = u_2, \quad \psi_1 = 0 \quad \text{on} \quad y = 0, \quad \psi_2 = Q_1 \quad \text{on} \quad y = h^+ \tag{19}$$

in $0 \le x \le 1$ and

$$\frac{\partial \psi_3}{\partial y} = u_3, \quad \psi_3 = 0 \quad \text{on} \quad y = 0 \tag{20}$$

in $1 \leq x \leq 1+\ell$, are given by

$$\psi_1 = \frac{Q_1 y^2(3h-2y) + hy(h-y)^2}{h^3}, \tag{21}$$

$$\psi_2 = Q_1 + \frac{Q_2(y-h)^2(3H-h-2y)}{(H-h)^3}, \tag{22}$$

$$\psi_3 = \frac{Q_3 y^2(3H-2y) + Hy(H-y)^2}{H^3}. \tag{23}$$

By global mass conservation we have

$$Q_1 + Q_2 = Q_3, \tag{24}$$

consistent with the fact that the wall $y = H$ comprises the streamline $\psi_2 = Q_1+Q_2$ in $0 \leq x \leq 1$ and the streamline $\psi_3 = Q_3$ in $1 \leq x \leq 1+\ell$.

From (3) the pressure in each region is independent of y. Assuming that pressure is continuous at the ends of the blade, so that

$$p_1(1) = p_2(1) = p_3(1) \quad (= p_L, \text{ say}) \tag{25}$$

and

$$p_1(0) = p_2(0) = p_3(1+\ell) \quad (= p_0, \text{ say}) \tag{26}$$

(where the periodicity of the array has been used), we have from (15) and (25)

$$p_1 = \frac{6}{\alpha}\left(\frac{1}{h_1} - \frac{1}{h}\right) - \frac{6Q_1}{\alpha}\left(\frac{1}{h_1^2} - \frac{1}{h^2}\right) + p_L, \tag{27}$$

$$p_2 = \frac{6Q_2}{\alpha}\left[\frac{1}{(H-h_1)^2} - \frac{1}{(H-h)^2}\right] + p_L, \tag{28}$$

$$p_3 = \frac{6(H-2Q_3)}{H^3}(x-1) + p_L. \tag{29}$$

Setting $x = 0$ in (27)–(28) and $x = 1+\ell$ in (29), and using (26), we obtain three representations of $p_0 - p_L$:

$$p_0 - p_L = \frac{6\left[Q_1(h_0+h_1) - h_0h_1\right]}{h_0^2 h_1^2}, \tag{30}$$

$$p_0 - p_L = \frac{6Q_2(2H-h_0-h_1)}{(H-h_0)^2(H-h_1)^2}, \tag{31}$$

$$p_0 - p_L = \frac{6\ell(H-2Q_3)}{H^3}. \tag{32}$$

Expressions for the Q_k ($k = 1, 2, 3$) and $p_0 - p_L$ obtained by solving (24) and (30)–(32) are given in equations (A1)–(A4) in the Appendix; from these it may be shown that $Q_k \geq 0$, as expected.

2.4. Moment of the forces on the blade

The moment of the forces (per unit length in the axial direction) on the blade about the pivot due to the pressure (non-dimensionalised with $\mu U L^3/h_{\rm p}^2$) is of the form $\mathbf{M} = M\mathbf{k}$, where

$$M = \int_0^1 (x - x_{\rm p})(p_1 - p_2)\,{\rm d}x. \tag{33}$$

For equilibrium of the blade we require $M = 0$, which leads to a lengthy equation, given as equation (A5) in the Appendix.

2.5. Transcendental equation for α

Elimination of Q_1, Q_2 and Q_3 between (A1)–(A5) leads to a lengthy algebraic transcendental equation of the form

$$F(\alpha, x_{\rm p}, H, \ell) = 0 \tag{34}$$

(omitted for brevity). This is the key result determining α when $x_{\rm p}$, H and ℓ are prescribed; then with α known, the complete solution (h_0, h_1, Q_k, u_k, p_k and ψ_k for $k = 1, 2, 3$) is determined. For all $x_{\rm p}$, H and ℓ equation (34) has the trivial solution $\alpha = 0$, corresponding to the blade being parallel to the walls, and therefore not acting as a scraper. We shall be concerned with the more interesting (nontrivial) solutions α of (34), which are of the general form

$$\alpha = \alpha(x_{\rm p}, H, \ell). \tag{35}$$

We note that if (35) is expressed in dimensional variables then it shows, rather unexpectedly, that α is independent of μ and U, and indeed is independent even of the *sign* of U.

In the case $\ell = 0$ region 3 is absent, $Q_1 = h_0 h_1/(h_0 + h_1)$, $Q_2 = 0$, and $p_0 = p_L$. Furthermore, in this case α is independent of H, because the fluid in region 2 is "shielded" from the moving boundary $y = 0$ by the blade $y = h$, and therefore plays no dynamical part — so the height of region 2 is irrelevant in determining α.

2.6. Solutions for α

The geometrical restrictions $h_0 > 0$, $h_0 < H$, $h_1 > 0$ and $h_1 < H$ mean respectively that $\alpha < \alpha_1(x_{\rm p})$, $\alpha > \alpha_2(x_{\rm p}, H)$, $\alpha > \alpha_3(x_{\rm p})$ and $\alpha < \alpha_4(x_{\rm p}, H)$, where

$$\alpha_1 = \frac{1}{x_{\rm p}}, \quad \alpha_2 = -\frac{H-1}{x_{\rm p}}, \quad \alpha_3 = -\frac{1}{1-x_{\rm p}}, \quad \alpha_4 = \frac{H-1}{1-x_{\rm p}}. \tag{36}$$

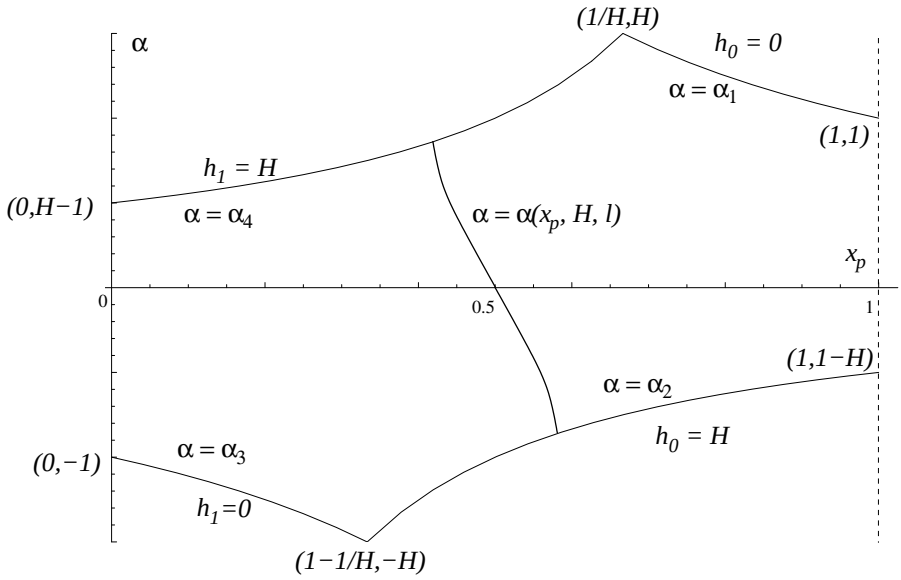

Figure 3. Sketch of the "allowed" region in the $(x_{\rm p}, \alpha)$ plane determined by (36) in which solutions $\alpha = \alpha(x_{\rm p}, H, \ell)$ of equation (34) may lie.

The general form of the region in the $(x_{\rm p}, \alpha)$ plane bounded by the curves (36) is sketched in Figure 3; the solution (35) can be physically meaningful only if it lies in this "allowed" region. As Figure 3 shows, the curves $\alpha = \alpha_1$ and $\alpha = \alpha_4$ intersect at $(x_{\rm p}, \alpha) = (1/H, H)$, and the curves $\alpha = \alpha_2$ and $\alpha = \alpha_3$ intersect at $(x_{\rm p}, \alpha) = (1 - 1/H, -H)$.

Any solution α of (34) is an odd function of $x_{\rm p} - \frac{1}{2}$, and so solution curves in the $(x_{\rm p}, \alpha)$ plane are skew-symmetric with respect to the point $(x_{\rm p}, \alpha) = (\frac{1}{2}, 0)$. In particular, nontrivial solutions satisfy

$$\alpha = C\left(x_{\rm p} - \tfrac{1}{2}\right) + O\left(x_{\rm p} - \tfrac{1}{2}\right)^3 \quad \text{as} \quad x_{\rm p} \to \tfrac{1}{2}, \tag{37}$$

where

$$C = -\frac{10(H-1)[(1+\ell)H^2 - 3\ell H + 6\ell]}{(1+\ell)H^3 - (1+4\ell)H^2 + 8\ell H - 7\ell}. \tag{38}$$

For future reference we note that C, the slope of this solution at $x_{\rm p} = \frac{1}{2}$, is positive for $1 < H < H_0$, negative for $H > H_0$, and infinite when $H = H_0$, where $H_0 = H_0(\ell)$ is the (unique) real positive zero of $(1+\ell)H^3 - (1+4\ell)H^2 + 8\ell H - 7\ell$; this zero satisfies $1 < H_0 < H_{\rm c}$, where $H_{\rm c} \simeq 1.7152$ is the unique real positive zero of $H^3 - 4H^2 + 8H - 7$. Correspondingly, if $H \geq H_{\rm c}$ then C is negative for any $\ell > 0$, whereas

if $1 < H < H_c$ then C is negative if $\ell < \ell_0$, infinite if $\ell = \ell_0$, and positive if $\ell > \ell_0$, where $\ell_0(H) = H^2(1-H)/(H^3 - 4H^2 + 8H - 7)$. In the special case $\ell = 0$ we have $C = -10$, independent of H.

Figure 4 shows the solutions α of equation (34) plotted as functions of x_p for several values of ℓ in each of the cases $H = \frac{3}{2}$, 2, 3; the bounding curves (36) (which depend on H but not ℓ) are also shown in each case. The solution curves in Figure 4 connect the bounding curves $\alpha = \alpha_2$ ($h_0 = H$) and $\alpha = \alpha_4$ ($h_1 = H$); however, despite appearances to the contrary in the case $\ell = \infty$ in Figure 4(c), they do *not* in general intersect the bounding curves $\alpha = \alpha_1$ ($h_0 = 0$) and $\alpha = \alpha_3$ ($h_1 = 0$), consistent with the fact that contact between the blade and the moving wall $y = 0$ (but not the stationary wall $y = H$) would lead to force singularities (see section 3).

As Figure 4 shows, it is found that the solution (35) exists only for x_p lying in some interval $x_{p,\min} \le x_p \le x_{p,\max}$ around $x_p = \frac{1}{2}$, where $x_{p,\min}$ and $x_{p,\max}$ ($= 1 - x_{p,\min}$) depend on the values of H and ℓ. In Figure 4(c) the solution α is determined uniquely by x_p on each solution curve (that is, for each ℓ), whereas in Figures 4(a) and 4(b) some of the solution curves are "sigmoidal", and there can be more than one solution α for a given value of x_p. This illustrates a general pattern, which we now describe.

As Figure 4 also shows, for each H all the (nontrivial) solution curves lie between the one for $\ell = 0$ (the leftmost one in $\alpha > 0$) and the one for $\ell = \infty$ (the rightmost one in $\alpha > 0$). For the case $\ell = 0$ the solution curve is independent of H, and α is a monotonic decreasing function of x_p, and so is determined uniquely by x_p. On the other hand, the character of the solution curve for the case $\ell = \infty$ changes with H. Figure 5 shows a sketch of the forms of the solution curve for $\ell = \infty$. Specifically, for $1 < H < H_c$ (where $H_c \simeq 1.7152$ is the critical value of H discussed above) the solution α is a monotonic increasing function of x_p; for $H = H_c$ the solution curve has infinite slope $\mathrm{d}\alpha/\mathrm{d}x_p$ at $x_p = \frac{1}{2}$; for $H_c < H < 2$ there are two points on the solution curve where the slope is infinite, and there are multiple solutions α for some x_p; for $H = 2$ the solution curve has infinite slope where it meets the bounding curves (36), at the points $(\frac{1}{2}, \pm 2)$; for $2 < H < H_c' \simeq 2.4032$ there are four points where the solution curve has infinite slope; for $H = H_c'$ these points coalesce pairwise, giving only two points where the slope is infinite; and for $H > H_c'$ the solution α is a monotonic decreasing function of x_p. Thus for $\ell = \infty$ there can be (depending on the value of H) up to three nontrivial solutions α for a given x_p in $x_{p,\min} \le x_p \le x_{p,\max}$, that is, there can be up to three equilibrium blade positions, each giving rise to a different flow pattern; a similar statement can be made in cases when ℓ is finite but sufficiently large.

(a)

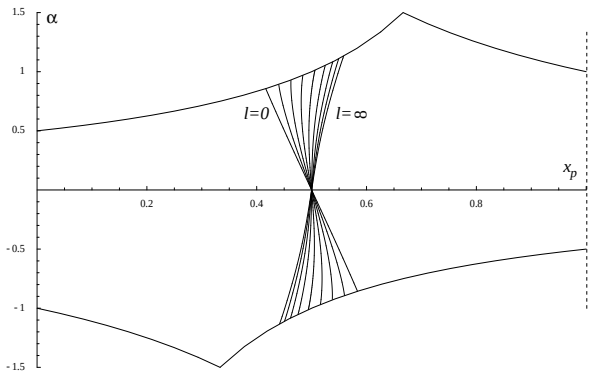

(b)

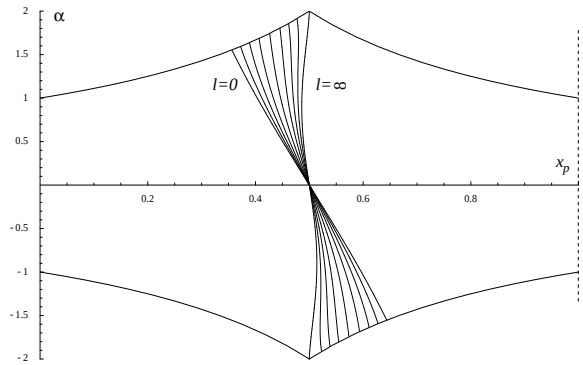

(c)

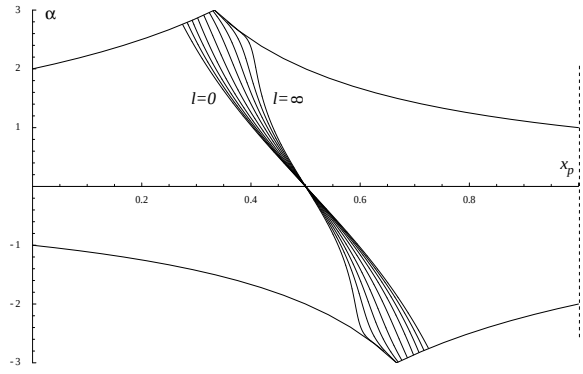

Figure 4. Plots of the solutions α of equation (34) as functions of $x_{\rm p}$ in the cases (a) $H = \frac{3}{2}$, (b) $H = 2$, and (c) $H = 3$, for $\ell = 0$, 0.1, 0.25, 0.5, 1, 2, 4, 10, ∞ in each case.

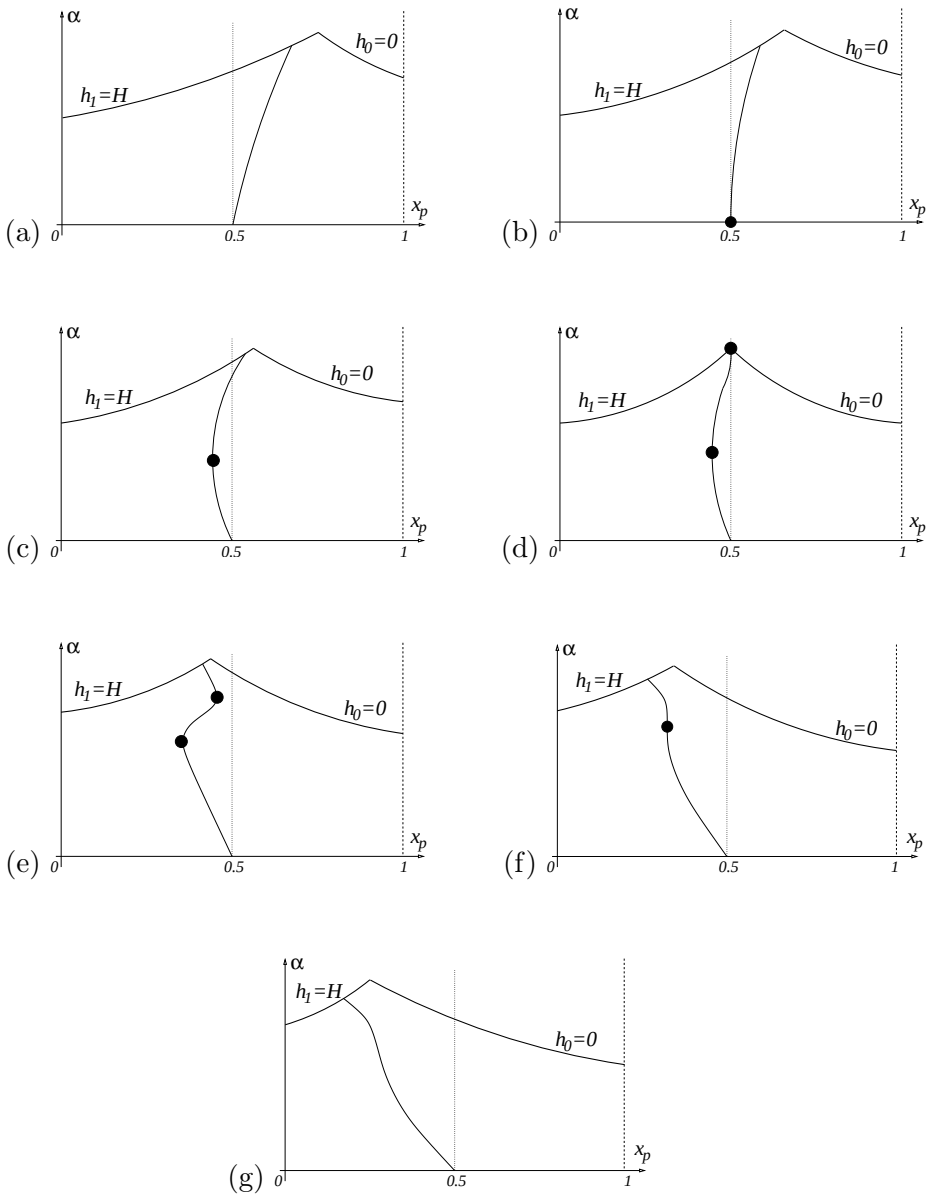

Figure 5. Sketch of the forms of the solution curve for $\ell = \infty$ in the upper half of the (x_p, α) plane for different values of H: (a) $1 < H < H_\mathrm{c}$, (b) $H = H_\mathrm{c} \simeq 1.7152$, (c) $H_\mathrm{c} < H < 2$, (d) $H = 2$, (e) $2 < H < H'_\mathrm{c}$, (f) $H = H'_\mathrm{c} \simeq 2.4032$, and (g) $H > H'_\mathrm{c}$. The dots indicate points where $\mathrm{d}\alpha/\mathrm{d}x_\mathrm{p} = \infty$.

(a)

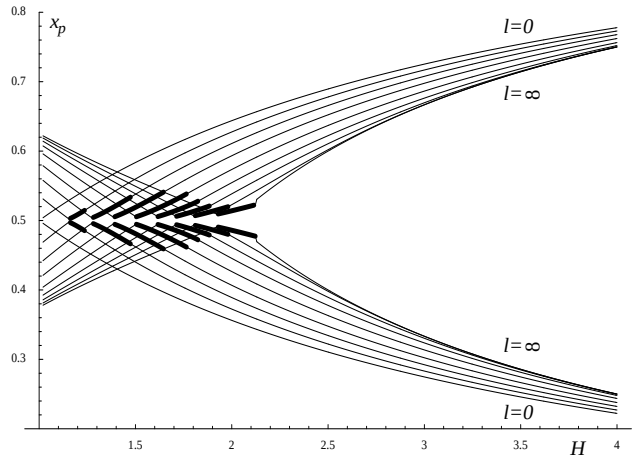

(b)

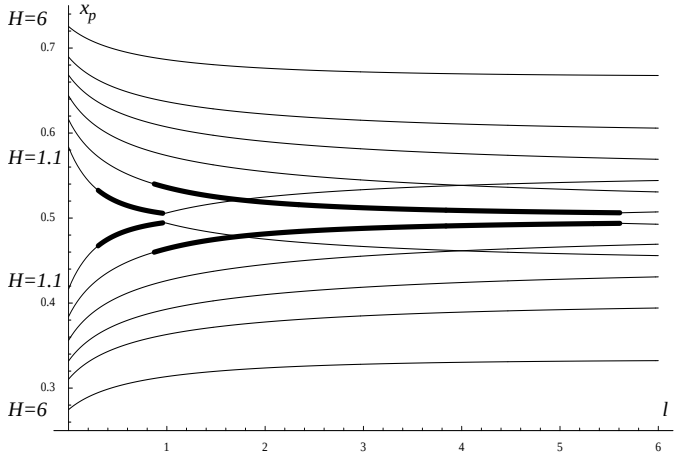

Figure 6. Plots of $x_{\mathrm{p,min}}$ and $x_{\mathrm{p,max}}$ (a) as functions of H for $\ell = 0$, 0.1, 0.25, 0.5, 1, 2, 4, 10, ∞, and (b) as functions of ℓ for $H = 1.1$, 1.5, 2, 3, 6. The thin curves correspond to cases where an end of the blade is in contact with the upper wall $y = H$ of the channel, so that $\alpha = \alpha_2(x_{\mathrm{p}})$ or $\alpha = \alpha_4(x_{\mathrm{p}})$; the thick curves correspond to cases where the minimum and maximum values of x_{p} occur with the blade away from the channel walls.

Figure 6 shows $x_{\mathrm{p,min}}$ and $x_{\mathrm{p,max}}$ plotted as functions of H for various values of ℓ, and as functions of ℓ for various values of H. When the solution α is a monotonic function of x_{p} the values of $x_{\mathrm{p,min}}$ and $x_{\mathrm{p,max}}$ are determined by the intersections of the solution curve with the bounding curves $\alpha = \alpha_2$ and $\alpha = \alpha_4$; these cases are shown as thin curves in Figure 6. When the solution α is a multivalued function of x_{p} the values of $x_{\mathrm{p,min}}$ and $x_{\mathrm{p,max}}$ are determined as positions x_{p} where $\mathrm{d}\alpha/\mathrm{d}x_{\mathrm{p}} = \infty$; these cases are shown as thick curves in Figure 6.

2.7. Qualitative features of the flow

Armed with the solution given above we can now describe all of the qualitative features of the flow.

Figures 7 and 8 show the fluxes Q_1 and Q_2 plotted as functions of x_{p} for $H = \frac{3}{2}$ and 3, respectively, for several values of ℓ in each case; the flux Q_3 (not shown for brevity) is then given by (24). Cases in which the Q_k are multivalued as functions of x_{p} correspond to cases in which the x_{p}-α relation is multivalued.

In region 3 the flow is rectilinear, with streamlines parallel to the channel walls. Equation (31) shows that $p_0 > p_L$, so that $Q_3 < \frac{1}{2}H$ and $p_{3x} > 0$ (that is, the pressure gradient is always adverse) and so backflow may occur. Specifically, from (18) the position $y = y_{03} \neq H$ where $u_3 = 0$ is given by

$$y_{03} = \frac{H^2}{3(H - 2Q_3)} = \text{constant}, \tag{39}$$

and the position $y = y_{\mathrm{m3}}$ where $u_{3y} = 0$ is given by

$$y_{\mathrm{m3}} = \frac{H(2H - 3Q_3)}{3(H - 2Q_3)} = \text{constant}; \tag{40}$$

thus $0 < y_{03} < H$ and $0 < y_{\mathrm{m3}} < H$ (that is, there is backflow near the upper wall $y = H$ in region 3) whenever $Q_3 < \frac{1}{3}H$.

In region 1 the pressure gradient p_{1x} may change sign, and backflow may again occur. Specifically, $u_1 = 0$ not only on the blade $y = h$ but also on the curve $y = y_{01}(x)$, where

$$y_{01} = \frac{h^2}{3(h - 2Q_1)}, \tag{41}$$

in the region where $h \geq 3Q_1$; such a region exists if h_0, h_1, Q_1 and α are such that $h_0 > 3Q_1$ (if $\alpha < 0$) or $h_1 > 3Q_1$ (if $\alpha > 0$). In that case the curve (41) meets the blade $y = h$ at the point where $h = 3Q_1$, which

(a)

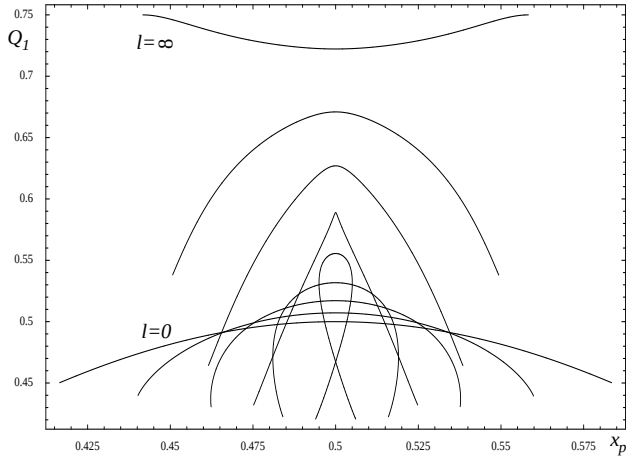

(b)

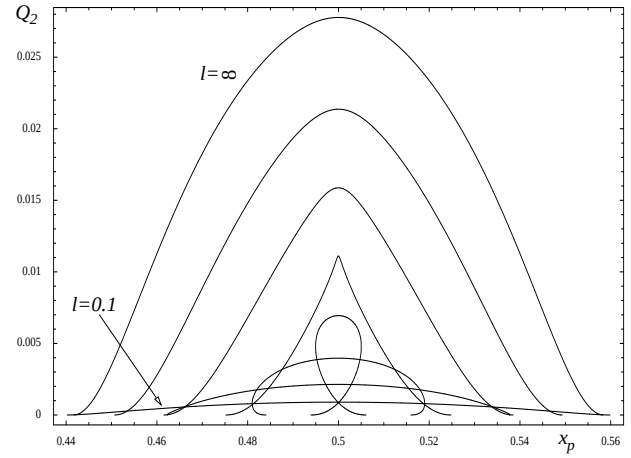

Figure 7. Plots of the fluxes (a) Q_1 and (b) Q_2 as functions of $x_{\rm p}$ in the case $H = \frac{3}{2}$, for $\ell = 0$, 0.1, 0.25, 0.5, 1, 2, 4, 10, ∞ (except that for the sake of clarity the curve $Q_2 = 0$ for $\ell = 0$ is not shown).

is a separation point; the separating streamline $y = y_{\rm s}(x)$ is given by $\psi_1 = Q_1$, leading to

$$y_{\rm s} = \frac{Q_1 h}{h - 2Q_1} \quad (< y_{01}). \tag{42}$$

(a)

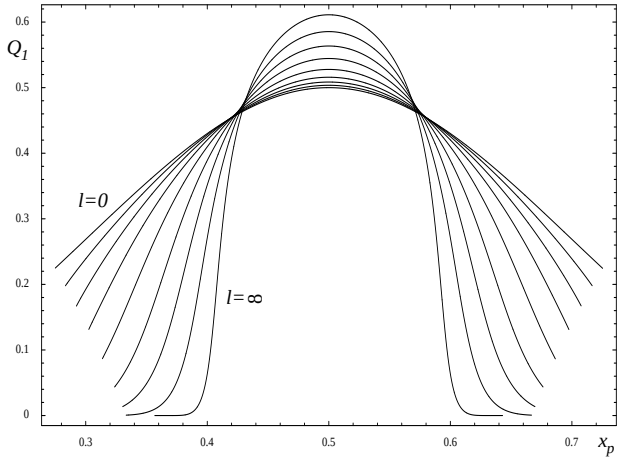

(b)

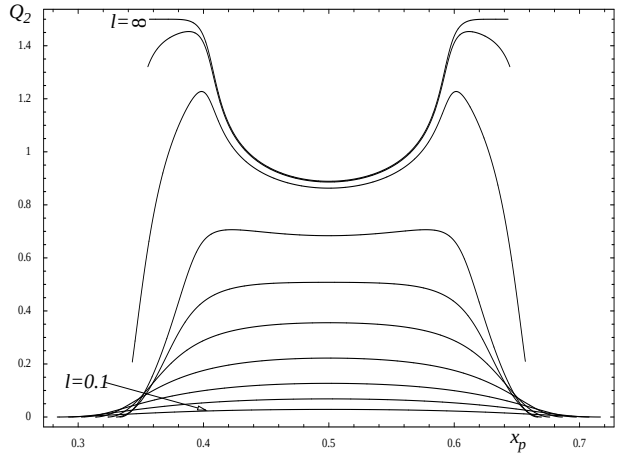

Figure 8. As in Figure 7, but with $H = 3$ and (a) $\ell = 0$, 0.1, 0.25, 0.5, 1, 2, 4, 10, ∞, (b) $\ell = 0.1$, 0.25, 0.5, 1, 2, 4, 10, 10^2, 10^3, ∞.

Also the curve $y = y_{\mathrm{m1}}(x)$ where $u_{1y} = 0$ is given by

$$y_{\mathrm{m1}} = \frac{h(2h - 3Q_1)}{3(h - 2Q_1)}. \tag{43}$$

Since $Q_2 \geq 0$, equations (15) and (17) show that $p_{2x} \leq 0$ (that is, the pressure gradient is always favourable), and u_2 (which is symmetric about $y = \frac{1}{2}(h + H)$) satisfies $u_2 \geq 0$ for all x, meaning that backflow never occurs in region 2.

(a)

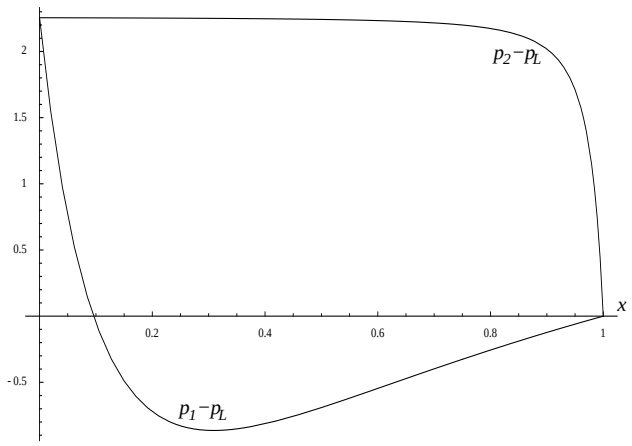

(b)

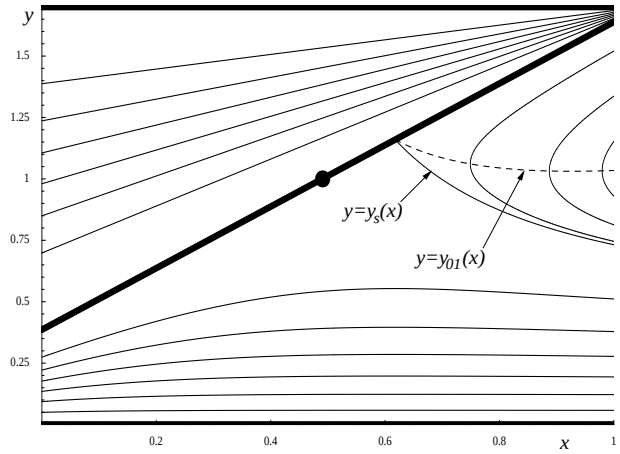

(c)

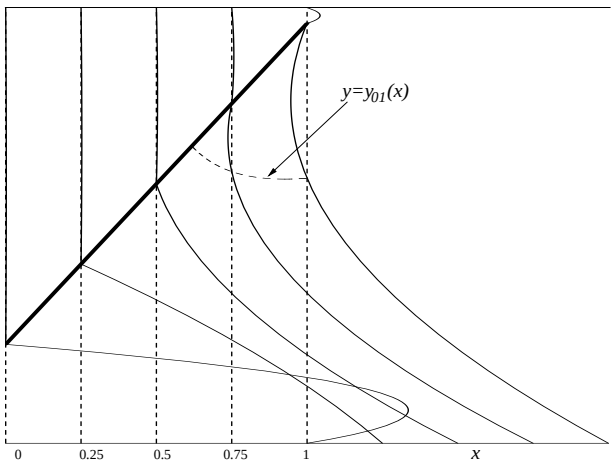

Figure 9. Plots of (a) the pressures $p_1 - p_L$ and $p_2 - p_L$ as functions of x, (b) corresponding streamline patterns, and (c) velocity profiles at some stations x in regions 1 and 2, in the case $H = 1.7$, $\ell = 2$, $x_{\rm p} = 0.49$ and $\alpha = 1.25322$. In (b) the dot denotes the pivot position.

(a)

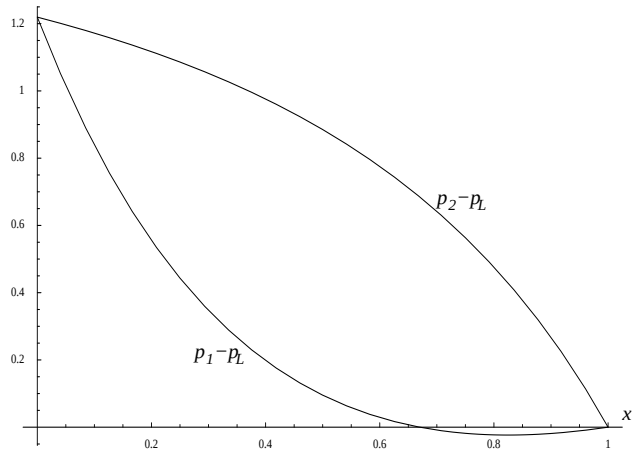

(b)

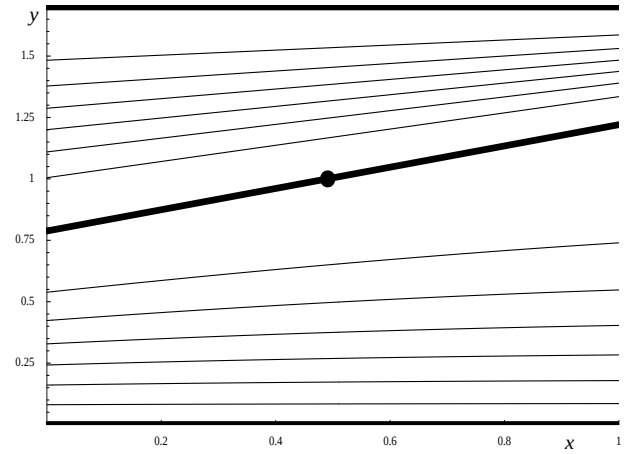

(c)

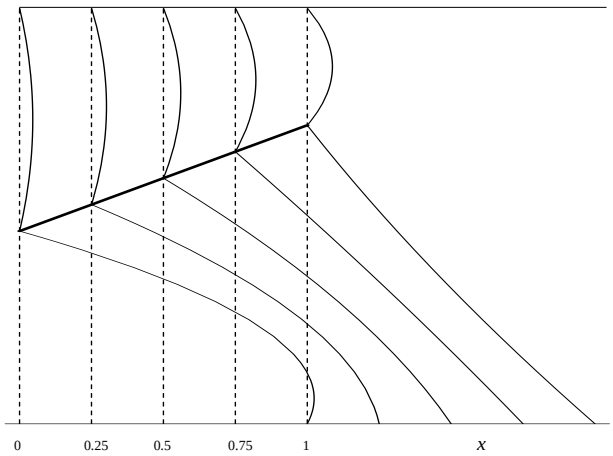

Figure 10. As in Figure 9, but with $H = 1.7$, $\ell = 2$, $x_{\mathrm{p}} = 0.49$ and $\alpha = 0.432872$.

(a)

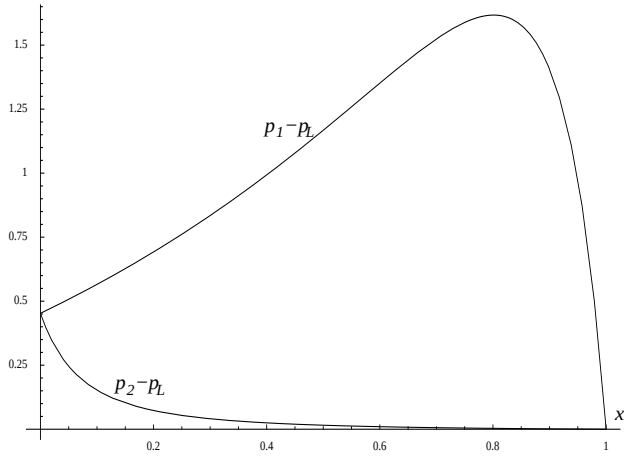

(b)

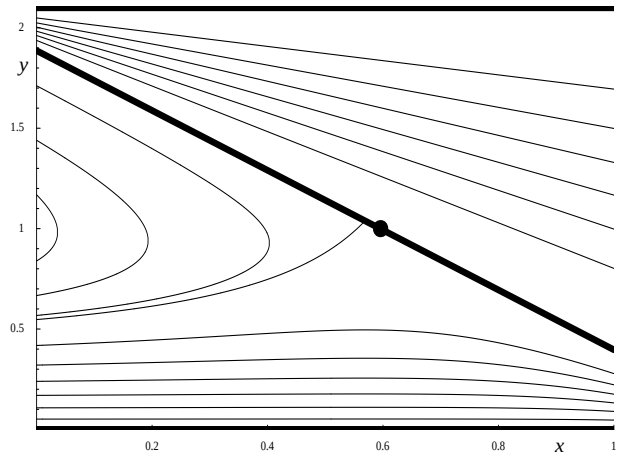

(c)

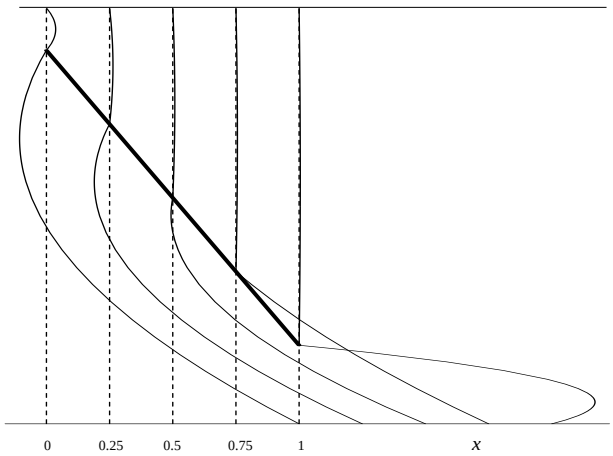

Figure 11. As in Figure 9, but with $H = 2.1$, $\ell = \frac{1}{2}$, $x_{\rm p} = 0.595$ and $\alpha = -1.48967$.

Figures 9–11 show, for various values of $x_{\rm p}$, H and ℓ, plots of the pressures $p_1 - p_L$ and $p_2 - p_L$ and the streamline patterns of the associated flows, together with examples of velocity profiles at various stations in regions 1 and 2. In particular, Figure 9 shows examples of the curves $y = y_{01}$ and $y = y_{\rm s}$ given by (41) and (42), respectively. Since the pressure $p_3 - p_L$ merely increases linearly with x across region 3 in accordance with (29) and the flow in region 3 is rectilinear, the corresponding plots in this region are omitted for brevity.

Figure 9 shows a case in which the pressure gradient p_{1x} is adverse near the trailing edge of the blade, so much so that there is backflow in region 1 there; similarly Figure 11 shows a case with backflow near the leading edge in region 1, whereas Figure 10 shows a case with no backflow. Also in each case it may be seen that if the gap between the blade and the moving wall $y = 0$ is sufficiently narrow then the maximum fluid velocity in region 1 can exceed the velocity of the moving wall.

The examples shown in Figures 9 and 10 were also chosen to demonstrate that two very different solutions are possible with the same values of the prescribed parameters, namely $x_{\rm p} = 0.49$, $H = 1.7$ and $\ell = 2$. With these parameter values the solution curve in the $(x_{\rm p}, \alpha)$ plane is somewhat like that sketched in Figure 5c, and equation (34) has two solutions α; Figure 9 is plotted for the solution $\alpha = 1.25322$, whereas Figure 10 is plotted for the solution $\alpha = 0.432872$.

Finally, we note that parabolic velocity profiles of the type (16)–(18), shown in Figures 9–11, are in broad agreement with experimental results obtained by MRI on an "idealized" SSHE geometry (Wang *et al.* [5]).

2.8. Forces on the blade and on the walls

The drag F_x and lift F_y on the blade, that is, the forces (per unit length in the axial direction) in the x and y directions acting on it due to the fluid (non-dimensionalised with $\mu UL/h_{\rm p}$ and $\mu UL^2/h_{\rm p}^2$, respectively), are given by

$$F_x = -\int_0^1 \left(\frac{\partial u_1}{\partial y} - \frac{\partial u_2}{\partial y}\right)_{y=h} {\rm d}x - \alpha \int_0^1 (p_1 - p_2)\,{\rm d}x \qquad (44)$$

and

$$F_y = \int_0^1 (p_1 - p_2)\,{\rm d}x, \qquad (45)$$

which lead to

$$F_x = \frac{6Q_1}{h_1^2} + \frac{6Q_2}{(H-h_1)^2} - \frac{6}{h_1} + \frac{4}{\alpha}\log\frac{h_1}{h_0} \qquad (46)$$

and

$$F_y = \frac{6Q_1}{h_0 h_1^2} - \frac{6Q_2}{(H-h_0)(H-h_1)^2} + \frac{6}{\alpha h_1} - \frac{6}{\alpha^2}\log\frac{h_1}{h_0}. \qquad (47)$$

The force (per unit length in the axial direction) in the x direction on the portion $0 \le x \le 1+\ell$ of the lower wall $y = 0$ due to the fluid (also non-dimensionalised with $\mu UL/h_{\rm p}$) is

$$F_0 = \int_0^1 \left.\frac{\partial u_1}{\partial y}\right|_{y=0} {\rm d}x + \int_1^{1+\ell} \left.\frac{\partial u_3}{\partial y}\right|_{y=0} {\rm d}x, \qquad (48)$$

which leads to

$$F_0 = \frac{6Q_1}{h_0 h_1} - \frac{4}{\alpha}\log\frac{h_1}{h_0} + \frac{2\ell(3Q_3 - 2H)}{H^2}, \qquad (49)$$

and the force (per unit length in the axial direction) in the x direction on the portion $0 \le x \le 1+\ell$ of the upper wall $y = H$ due to the fluid (also non-dimensionalised with $\mu UL/h_{\rm p}$) is

$$F_H = -\int_0^1 \left.\frac{\partial u_2}{\partial y}\right|_{y=H} {\rm d}x - \int_1^{1+\ell} \left.\frac{\partial u_3}{\partial y}\right|_{y=H} {\rm d}x, \qquad (50)$$

which leads to

$$F_H = \frac{6Q_2}{(H-h_0)(H-h_1)} + \frac{2\ell(3Q_3 - H)}{H^2}. \qquad (51)$$

As a check on the correctness of these expressions we note that the total force (per unit length in the axial direction) in the x direction acting on the fluid in $0 \le x \le 1+\ell$, $0 \le y \le H$, namely $-F_x - F_0 - F_H$, is identically zero, as it should be.

Figure 12 shows the force F_0 plotted as a function of $x_{\rm p}$ for $H = \frac{3}{2}$ and various values of ℓ, and Figure 13 shows F_0 plotted as a function of $x_{\rm p}$ for $\ell = 100$ and various values of H. (The corresponding plots of the forces F_x, F_y and F_H are omitted for brevity.) Each of the plots of F_0 is symmetric about a maximum at $x_{\rm p} = \frac{1}{2}$, and the numerical results indicate that, in general, the larger the value of ℓ, the larger $|F_0|$ is.

The pivot must exert forces $-F_x$ and $-F_y$ on the blade in order to maintain its equilibrium; similarly, forces $-F_0$ and $-F_H$ must be exerted on the walls $y = 0$ and $y = H$ respectively to maintain the flow. Dimensional estimates of the torque and power (per unit length in the axial direction) required to turn the rotor of the SSHE are therefore provided by $-NF_0R_1$ and $-NF_0U$ respectively, where again R_1 is the radius of the rotor and $N = 2\pi R_1/(L+\ell)$ is the number of blades.

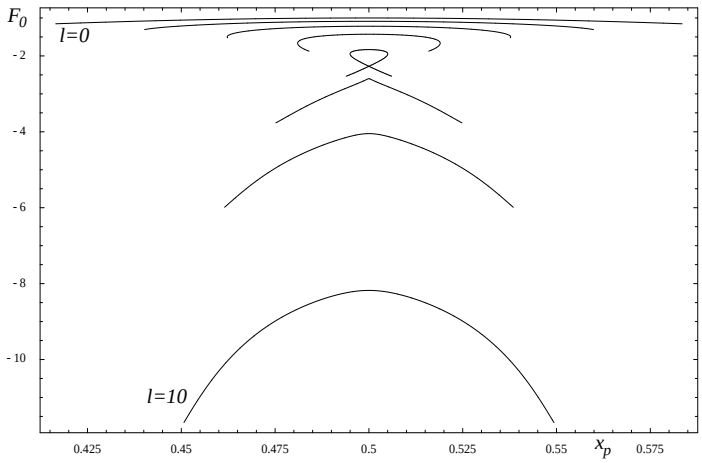

Figure 12. Plots of the force F_0 on the lower wall $y = 0$ as a function of x_p in the case $H = \frac{3}{2}$, for $\ell = 0$, 0.1, 0.25, 0.5, 1, 2, 4, 10.

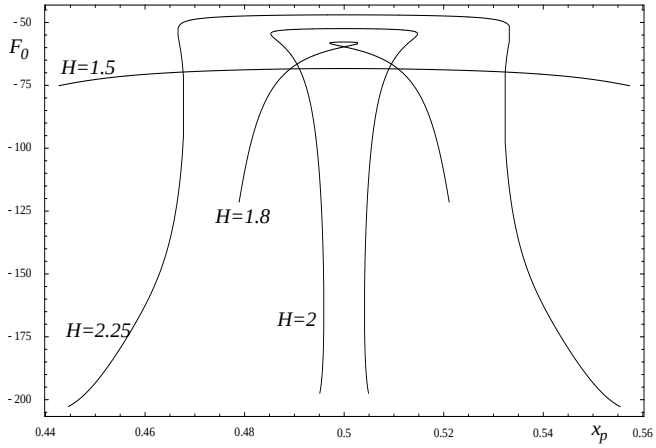

Figure 13. Plots of the force F_0 on the lower wall $y = 0$ as a function of x_p in the case $\ell = 100$, for $H = 1.5$, 1.8, 2, 2.25.

3. Contact between the blade and a channel wall

As described in subsection 2.6, equation (34) (which determines the possible equilibrium positions of a blade that is *not* in contact with a wall of the channel) has nontrivial solutions α only when x_p is sufficiently close to $\frac{1}{2}$. In practice, however, the pivot position of a typical SSHE blade is near the right-hand end of the blade (so that $x_\mathrm{p} \simeq 1$), and so equation (34) has no solution, that is, there is *no* equilibrium

position of the type considered available for the blade. We conclude that in such a case one of the ends of the blade makes contact with a wall of the channel. This is exactly what is wanted in practice, but it means that we must modify our analysis leading to (34) to allow for blade contact.

3.1. A Newtonian fluid with no slip

Suppose that the blade touches the moving wall $y = 0$ at the left-hand end $x = 0$, so that $h_0 = 0$, and as a consequence $Q_1 = 0$ and $Q_2 = Q_3 = Q$, say. The blade could alternatively contact the walls at $x = 0$, $y = H$, at $x = 1$, $y = 0$, or at $x = 1$, $y = H$, but these cases are of less relevance to a real SSHE, and so we will not consider them, except to say that the solution for a case when the blade *just* touches the *stationary* wall $y = H$ may be obtained simply by taking the appropriate (regular) limit of the results in section 2.

We again take the blade to be given by $y = h(x)$, but now with

$$h(x) = \alpha x \quad (\alpha > 0), \tag{52}$$

and with α regarded as prescribed. Equations (3)–(32) again hold (with $h_0 = 0$, $Q_1 = 0$, and $h_1 = \alpha < H$), except that (26) must be replaced by

$$p_2(0) = p_3(1 + \ell) \quad (= p_0, \text{ say}), \tag{53}$$

and the result (30) must be dropped. Moreover the moment M in (33) can no longer be prescribed (and, in particular, will no longer vanish, in general).

Equations (31) and (32) lead to

$$Q = \frac{\alpha\ell H(H-\alpha)^2}{(2\alpha\ell - H)(H-\alpha)^2 + H^3} \tag{54}$$

and

$$p_0 - p_L = \frac{6\alpha\ell(2H-\alpha)}{H[(2\alpha\ell - H)(H-\alpha)^2 + H^3]}. \tag{55}$$

The velocities and pressures are then given by (16)–(18) and (27)–(29), respectively. Figure 14 shows an example of the pressures $p_1 - p_L$ and $p_2 - p_L$ plotted as functions of x. We note from (15) that $p_{1x} > 0$, and from (54) that $Q > 0$ and $Q < \frac{1}{2}H$, so that $p_{2x} < 0$ and $p_{3x} > 0$. Equation (16) shows that there is backflow in the region $0 \le y \le h$ under the blade, with $u_{1y} = 0$ on $y = y_{\mathrm{m}1} = \frac{2}{3}h$ and $u_1 = 0$ on $y = y_{01} = \frac{1}{3}h$. Also y_{03} and $y_{\mathrm{m}3}$ in (39) and (40) are given by

$$y_{03} = \frac{H}{3} + \frac{2\ell(H-\alpha)^2}{3(2H-\alpha)} > \frac{H}{3} \tag{56}$$

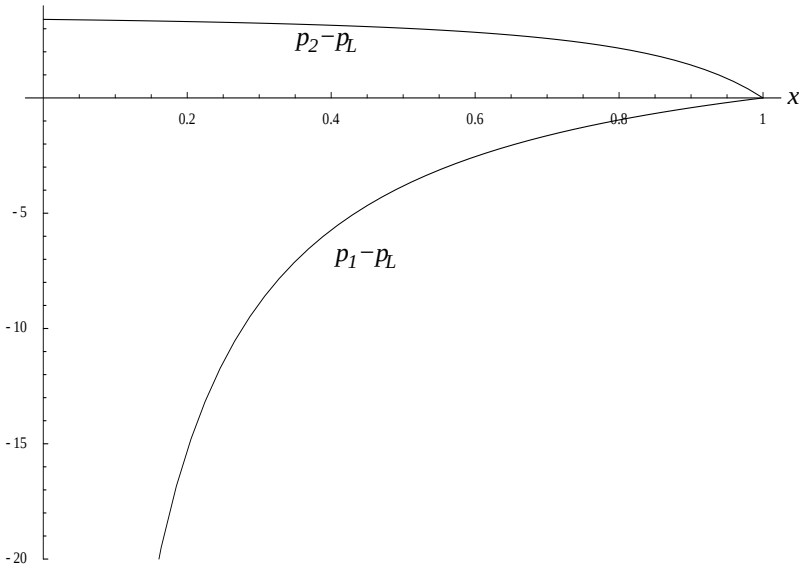

Figure 14. Plot of the pressures $p_1 - p_L$ and $p_2 - p_L$ as functions of x, in the case $H = 1.7$, $\ell = 2$, $\alpha = 1.25322$, when the blade is in contact with the moving wall $y = 0$ at $x = 0$.

and

$$y_{\mathrm{m}3} = \frac{2H}{3} + \frac{\ell(H-\alpha)^2}{3(2H-\alpha)} > \frac{2H}{3}, \tag{57}$$

so that $y_{03} < H$ and $y_{\mathrm{m}3} < H$ (that is, there is backflow near $y = H$ in region 3) only for sufficiently small ℓ.

However, this solution has a major shortcoming: equations (16) and (27) show that in the limit $x \to 0$ (so that $h = \alpha x \to 0$)

$$\left.\frac{\partial u_1}{\partial y}\right|_{y=0} = -\frac{4}{\alpha x} \to -\infty, \quad \left.\frac{\partial u_1}{\partial y}\right|_{y=h} = \frac{2}{\alpha x} \to \infty, \quad p_1 \sim -\frac{6}{\alpha^2 x} \to -\infty \tag{58}$$

(the latter being evident in Figure 14), the forces F_x, F_y and F_0 are infinite, and there is an infinite moment M on the blade about a pivot at $x = x_{\mathrm{p}}$ tending to keep it in contact with the wall.

In reality the stresses near the contact point $x = 0$, $y = 0$ may become large, but will, of course, remain finite; the singularities predicted above are a consequence of the simplifying assumptions concerning the two-dimensional nature of the problem, and the interaction between, and the nature of, the fluid, the blade and the moving wall.

Various alternative modelling assumptions may be invoked to alleviate these singularities; in particular, as we shall show, allowing

non-Newtonian fluid behaviour, slip at solid boundaries, or cavitation in regions of low pressure can achieve this. Which (if any) of these effects is most significant in practice remains an interesting open question. Precedents for these sorts of approach were established by, for example, Silliman and Scriven [17], who showed that slip can alleviate the stress singularity occurring in viscous flow at a channel exit, and Weidner and Schwartz [18], who showed that non-Newtonian (power-law) behaviour can alleviate the stress singularity at a three-phase contact line moving over a solid substrate; it is well known that slip at the substrate can have a similar effect.

3.2. A POWER-LAW FLUID

Consider an incompressible shear-thinning power-law fluid, with dimensional constitutive equation

$$\boldsymbol{\sigma} = 2\mu(q)\mathbf{e}, \quad \mu(q) = \mu_0 q^{n-1}, \quad q = (2\,\mathrm{tr}\,(\mathbf{e}^2))^{1/2}, \tag{59}$$

where $\boldsymbol{\sigma}$ is the partial-stress tensor, $\mathbf{e}$ is the rate-of-strain tensor, q is the local shear rate, and μ_0 and n (< 1) are constants. Non-dimensionalising as before using $\mu_0(U/h_\mathrm{p})^{n-1}$ in place of μ for such a fluid the lubrication approximation gives (see, for example, Johnson and Mangkoesoebroto [19] and Ross, Wilson and Duffy [20])

$$\frac{\partial}{\partial y}\left(q_k^{n-1}\frac{\partial u_k}{\partial y}\right) = \frac{\partial p_k}{\partial x}, \quad \frac{\partial p_k}{\partial y} = 0, \quad \frac{\partial u_k}{\partial x} + \frac{\partial v_k}{\partial y} = 0, \quad q_k = \left|\frac{\partial u_k}{\partial y}\right| \tag{60}$$

for $k = 1, 2, 3$, to be solved subject to (4), (5), (25) and (53). Again we take h to have the form (52), and so again we have $Q_1 = 0$ and $Q_2 = Q_3 = Q$.

Solving (60) is rather more tedious than solving (3), because more care must be taken with the signs of velocity gradients in different parts of the flow domain. For example, to determine the solution in region 1 we recall that $y = y_{\mathrm{m}1}(x)$ is the curve on which $u_{1y} = 0$ (with $0 < y_{\mathrm{m}1} < h$, since $Q_1 = 0$), so that $u_{1y} < 0$ in $y < y_{\mathrm{m}1}$ and $u_{1y} > 0$ in $y > y_{\mathrm{m}1}$. We then solve for u_1 in $0 \le y \le y_{\mathrm{m}1}$ and $y_{\mathrm{m}1} \le y \le h$ separately, and equate expressions for u_1 at $y = y_{\mathrm{m}1}$ to obtain one relation between $y_{\mathrm{m}1}$ and the pressure gradient p_{1x}. A second relation between $y_{\mathrm{m}1}$ and p_{1x} is found by using the fact that $Q_1 = 0$. From these two relations it is found that the curve $y = y_{\mathrm{m}1}(x)$ is, in fact, a straight line $y = b\alpha x$, where the constant b ($\frac{1}{2} < b < 1$) is a solution of the equation

$$(n + 1 + nb)(1 - b)^{\frac{n+1}{n}} = nb^{\frac{2n+1}{n}}. \tag{61}$$

Also

$$u_1 = \frac{|y - y_{\rm m1}|^{\frac{n+1}{n}} - (h - y_{\rm m1})^{\frac{n+1}{n}}}{y_{\rm m1}^{\frac{n+1}{n}} - (h - y_{\rm m1})^{\frac{n+1}{n}}}, \tag{62}$$

or equivalently

$$u_1 = \left(1 + \frac{nb}{n+1}\right)\left|\frac{y}{bh} - 1\right|^{\frac{n+1}{n}} - \frac{nb}{n+1}; \tag{63}$$

the curve $y = y_{01}$ ($< y_{\rm m1}$) on which $u_1 = 0$ is found to satisfy

$$y_{\rm m1} = \tfrac{1}{2}(h + y_{01}). \tag{64}$$

The pressure p_1 is given by

$$p_1 = -\frac{b^n}{n\alpha(1-b)^{n+1}}\left(\frac{1}{h^n} - \frac{1}{\alpha^n}\right) + p_L. \tag{65}$$

A similar procedure for region 2 gives

$$u_2 = \frac{2n+1}{n+1}\frac{Q}{H-h}\left(1 - \left|\frac{h + H - 2y}{H-h}\right|^{\frac{n+1}{n}}\right) \tag{66}$$

(symmetric about $y = \frac{1}{2}(h + H)$),

$$p_2 = \frac{1}{n\alpha}\left(\frac{2(2n+1)Q}{n}\right)^n\left[\frac{1}{(H-\alpha)^{2n}} - \frac{1}{(H-h)^{2n}}\right] + p_L \tag{67}$$

and

$$p_0 - p_L = \frac{1}{n\alpha}\left(\frac{2(2n+1)Q}{n}\right)^n\left[\frac{1}{(H-\alpha)^{2n}} - \frac{1}{H^{2n}}\right], \tag{68}$$

with the flux Q an unknown constant.

The procedure for region 3 is more lengthy, because cases with and without backflow must be treated separately; it is found eventually that

$$u_3 = \frac{|y - y_{\rm m3}|^{\frac{n+1}{n}} - |H - y_{\rm m3}|^{\frac{n+1}{n}}}{y_{\rm m3}^{\frac{n+1}{n}} - |H - y_{\rm m3}|^{\frac{n+1}{n}}}, \tag{69}$$

$$p_3 = \left(\frac{n+1}{n}\right)^n \frac{1}{\left[y_{\rm m3}^{\frac{n+1}{n}} - |H - y_{\rm m3}|^{\frac{n+1}{n}}\right]^n}(x-1) + p_L \tag{70}$$

and

$$p_0 - p_L = \left(\frac{n+1}{n}\right)^n \frac{\ell}{\left[y_{\rm m3}^{\frac{n+1}{n}} - |H - y_{\rm m3}|^{\frac{n+1}{n}}\right]^n}, \tag{71}$$

where $y = y_{\rm m3}$ is again the position at which $u_{3y} = 0$. The flux Q satisfies

$$Q = \frac{n y_{\rm m3}^{\frac{2n+1}{n}} - [(n+1)H + n y_{\rm m3}]\,|H - y_{\rm m3}|^{\frac{n+1}{n}}}{(2n+1)\left[y_{\rm m3}^{\frac{n+1}{n}} - |H - y_{\rm m3}|^{\frac{n+1}{n}}\right]}. \tag{72}$$

Finally, elimination of Q and $p_0 - p_L$ between (68), (71) and (72) leads to an equation determining $y_{\rm m3}$:

$$n y_{\rm m3}^{\frac{2n+1}{n}} - [(n+1)H + n y_{\rm m3}]\,|H - y_{\rm m3}|^{\frac{n+1}{n}} = \frac{(n+1)(n\alpha\ell)^{\frac{1}{n}}}{2\left[(H-\alpha)^{-2n} - H^{-2n}\right]^{\frac{1}{n}}} \tag{73}$$

(which shows that $y_{\rm m3}$ is a constant, independent of x). It may be shown that for sufficiently small ℓ equation (73) has a solution $y_{\rm m3}$ satisfying $\frac{1}{2}H < y_{\rm m3} < H$, so there is backflow near $y = H$ in this case.

As a check on these results we note that in the case $n = 1$ the solution of (61) is $b = \frac{2}{3}$ (so that $y_{\rm m1} = \frac{2}{3}h$), and the solution $y_{\rm m3}$ of (73) is again (57); thus when $n = 1$ the results (62)–(72) for the velocities, pressures and fluxes reduce to those for a Newtonian fluid.

From (62) and (65) we find that the stresses in region 1 are $O(x^{-n})$ as $x \to 0$, and so are again singular; however, the singularities in this case are integrable for $n < 1$. Essentially the large shear rates near the contact point lead to a low viscosity there, and hence to stresses that, though singular, lead to finite forces and moment; specifically we find from (44), (45), (48) and (50) that the forces (per unit length in the axial direction) F_x, F_y, F_0 and F_H take the forms

$$F_x = \frac{\alpha^{-n}}{1-n}\left(\frac{b}{1-b}\right)^{n+1} + \frac{1}{n\alpha}\left(\frac{2(1+2n)Q}{n}\right)^n \times \left[\frac{\alpha}{(H-\alpha)^{2n}} + (1-n)\frac{(H-\alpha)^{1-2n} - H^{1-2n}}{1-2n}\right], \tag{74}$$

$$F_y = -\frac{\alpha^{-(1+n)}}{(1-n)b}\left(\frac{b}{1-b}\right)^{n+1} - \frac{1}{n\alpha^2}\left(\frac{2(1+2n)Q}{n}\right)^n \times \left[\frac{\alpha}{(H-\alpha)^{2n}} + \frac{(H-\alpha)^{1-2n} - H^{1-2n}}{1-2n}\right], \tag{75}$$

$$F_0 = -\frac{\alpha^{-n}}{1-n}\left(\frac{b}{1-b}\right)^{n+1} - \left(\frac{n+1}{n}\right)^n \frac{\ell y_{\rm m3}}{\left[y_{\rm m3}^{\frac{n+1}{n}} - |H - y_{\rm m3}|^{\frac{n+1}{n}}\right]^n}, \tag{76}$$

$$F_H = -\frac{1}{\alpha}\left(\frac{2(1+2n)Q}{n}\right)^n \frac{(H-\alpha)^{1-2n} - H^{1-2n}}{1-2n} - \left(\frac{n+1}{n}\right)^n \frac{\ell(H-y_{\rm m3})}{\left[y_{\rm m3}^{\frac{n+1}{n}} - |H-y_{\rm m3}|^{\frac{n+1}{n}}\right]^n} \tag{77}$$

(again satisfying $F_x + F_0 + F_H = 0$), and from (33) the moment of forces on the blade about a pivot at $x = x_{\rm p}$, $y = 1 = \alpha x_{\rm p}$ is

$$M = \frac{1}{2n\alpha^3}\left[\frac{n\alpha^{1-n}[2(2-n)-(1-n)\alpha]}{b(1-n)(2-n)}\left(\frac{b}{1-b}\right)^{n+1} + \left(\frac{2(1+2n)Q}{n}\right)^n \times \left\{\frac{\alpha(2-\alpha)}{(H-\alpha)^{2n}} - \frac{(H-\alpha)^{1-2n}[2(n-1)+H+(1-2n)\alpha] - H^{1-2n}[2(n-1)+H]}{(1-n)(1-2n)}\right\}\right]. \tag{78}$$

These quantities are finite for $n < 1$, but all except F_H are singular in the Newtonian limit $n \to 1^-$.

3.3. A Newtonian fluid with slip at boundaries

We now consider the case of a Newtonian fluid that may slip along the lower wall $y = 0$ and the lower face $y = h^-$ of the blade, with relative velocity proportional to the local shear rate (see, for example, Greenspan [21] and Hocking [22]); for simplicity we shall continue to assume that there is no slip at the upper surface $y = h^+$ of the blade and at the upper wall $y = H$ (though the analysis could be extended to include slip on these boundaries too, if desired).

Again we take h to have the form (52), and so again we have $Q_1 = 0$ and $Q_2 = Q_3 = Q$. The lubrication equations (3) must now be solved subject to (25), (53) and, in place of (4) and (5),

$$u_1 - 1 = \beta u_{1y} \quad \text{on} \quad y = 0, \quad u_1 = -\beta u_{1y} \quad \text{on} \quad y = h^-, \qquad u_2 = 0 \quad \text{on} \quad y = h^+, \quad u_2 = 0 \quad \text{on} \quad y = H \tag{79}$$

in $0 \le x \le 1$, and

$$u_3 - 1 = \beta u_{3y} \quad \text{on} \quad y = 0, \quad u_3 = 0 \quad \text{on} \quad y = H \tag{80}$$

in $1 \le x \le 1 + \ell$, where β (> 0) is a (small) non-dimensional slip length, taken to be the same for the two boundaries $y = 0$ and $y = h^-$. Although a slip length may in general be variable, here we shall for simplicity take β to be a constant.

These equations are solved in an analogous way to those in section 2. In particular, it is found that

$$u_1 = \frac{3(h+2\beta)y^2 - 4h(h+3\beta)y + h^2(h+4\beta)}{h(h+2\beta)(h+6\beta)}, \tag{81}$$

$$u_2 = \frac{6Q(H-y)(y-h)}{(H-h)^3}, \tag{82}$$

$$u_3 = \frac{[6Q\{(H+\beta)y + H\beta\} + H^2(H-3y)](H-y)}{H^3(H+4\beta)}, \tag{83}$$

and

$$p_1 = \frac{1}{\alpha\beta}\log\frac{h(\alpha+6\beta)}{\alpha(h+6\beta)} + p_L, \tag{84}$$

$$p_2 = \frac{6Q}{\alpha}\left[\frac{1}{(H-\alpha)^2} - \frac{1}{(H-h)^2}\right] + p_L, \tag{85}$$

$$p_3 = \frac{6[H^2 - 2Q(H+\beta)]}{H^3(H+4\beta)}(x-1) + p_L. \tag{86}$$

Setting $x = 0$ in (85) and $x = 1 + \ell$ in (86), and using (53), we obtain

$$p_0 - p_L = \frac{6Q(2H-\alpha)}{(H-\alpha)^2H^2} = \frac{6\ell[H^2 - 2Q(H+\beta)]}{H^3(H+4\beta)}, \tag{87}$$

which lead to

$$Q = \frac{\ell H^2(H-\alpha)^2}{2\ell(H-\alpha)^2(H+\beta) + H(2H-\alpha)(H+4\beta)} \tag{88}$$

and

$$p_0 - p_L = \frac{6\ell(2H-\alpha)}{2\ell(H-\alpha)^2(H+\beta) + H(2H-\alpha)(H+4\beta)}. \tag{89}$$

Equation (81) shows that there is backflow in the region $0 \le y \le h$ under the blade, with $u_{1y} = 0$ on $y = y_{\mathrm{m1}}$ and $u_1 = 0$ on $y = y_{01}$, where

$$y_{\mathrm{m1}} = \frac{2h(h+3\beta)}{3(h+2\beta)}, \quad y_{01} = \frac{h[2(h+3\beta) - (h^2 + 6h\beta + 12\beta^2)^{1/2}]}{3(h+2\beta)}. \tag{90}$$

The slip velocities on $y = 0$ and $y = h^-$ are

$$u_1|_{y=0} = 1 - \frac{4\beta(h+3\beta)}{(h+2\beta)(h+6\beta)}, \quad u_1|_{y=h^-} = -\frac{2h\beta}{(h+2\beta)(h+6\beta)}, \tag{91}$$

both of which vanish as the corner at $x = 0$ is approached. In region 2 the above results depend on the slip length β only via the value of Q.

From (88) we have $Q > 0$, so that $p_{2x} < 0$, and $Q < H^2/(2(H+\beta))$, so that $p_{3x} > 0$, as in the no-slip case. The positions $y = y_{03}$ where $u_3 = 0$ and $y = y_{\mathrm{m}3}$ where $u_{3y} = 0$ are again given by (56) and (57), independent of β.

As a check we note that when $\beta = 0$ the above results for the velocities, pressures and fluxes reduce to those in the no-slip case.

In the limit $x \to 0$ the viscous stresses are finite, but p_1 is singular:

$$p_1 \sim \frac{1}{\alpha\beta} \log \frac{(\alpha+6\beta)x}{6\beta} \to -\infty. \tag{92}$$

However, this singularity is integrable, and from (44), (45), (48), (50) and (33) we find that

$$F_x = \frac{6Q}{(H-\alpha)^2} + \frac{1}{\alpha} \log \frac{(\alpha+2\beta)(\alpha+6\beta)^3}{432\beta^4}, \tag{93}$$

$$F_y = -\frac{6Q}{H(H-\alpha)^2} - \frac{6}{\alpha^2} \log \frac{\alpha+6\beta}{6\beta}, \tag{94}$$

$$F_0 = -\frac{1}{\alpha} \log \frac{(\alpha+2\beta)(\alpha+6\beta)^3}{432\beta^4} + \frac{2\ell(3Q-2H)}{H(H+4\beta)}, \tag{95}$$

$$F_H = \frac{6Q}{H(H-\alpha)} + \frac{2\ell\left[3Q(H+2\beta) - H^2\right]}{H^2(H+4\beta)} \tag{96}$$

(again satisfying $F_x + F_0 + F_H = 0$), and

$$M = \frac{3}{\alpha^3}\left[\frac{Q(2H^2 - 3H\alpha + 2\alpha)\alpha}{H(H-\alpha)^2} + 2Q \log \frac{H-\alpha}{H} - \alpha + 2(1+3\beta) \log \frac{\alpha+6\beta}{6\beta}\right]. \tag{97}$$

These quantities are finite for $\beta > 0$, but all except F_H are singular in the no-slip limit $\beta \to 0$.

3.4. A Newtonian fluid with cavitation

Here we re-consider flow of a Newtonian fluid when there is blade contact at $x = 0$ (so that h has the form (52), and $Q_1 = 0$), but now we suppose that cavitation will occur in any region in which the pressure falls below a critical value p^* (which may be the vapour pressure of the process material, or the saturation pressure of any dissolved gases). In practice a SSHE is pressurized (up to, perhaps, 100 bar), and we will assume that the level of the internal pressure (measured by p_L) is sufficiently large that cavitation does not occur in regions 2 or 3; cavitation thus occurs only in region 1 where the fluid pressure would

otherwise become large and negative in the vicinity of $x = 0$ as shown in Figure 14.

Suppose that a cavitation "bubble" occupies the interval $0 \leq x \leq x^*$ in region 1 (with x^* unknown as yet), so that the pressure p_1 satisfies the boundary condition[2]

$$p_1 = p^* \quad \text{at} \quad x = x^*. \tag{98}$$

In fact, since the cavitation bubble is occupied by vapour (of low viscosity and density, presumably), we will assume both that the viscous stresses in the bubble may be neglected, and that p_1 takes the (uniform) value p^* throughout $0 \leq x \leq x^*$.

Except in the cavitation bubble the solution is exactly as described in subsection 3.1, and it is found from (27) (with $Q_1 = 0$) that

$$x^* = \left[1 + \frac{\alpha^2}{6}(p_L - p^*)\right]^{-1}. \tag{99}$$

The associated forces and moment are now finite; specifically, with

$$p_1 = p^*, \quad \left.\frac{\partial u_1}{\partial y}\right|_{y=0} = 0, \quad \left.\frac{\partial u_1}{\partial y}\right|_{y=h} = 0 \quad \text{in} \quad 0 \leq x \leq x^* \tag{100}$$

in (33), (44), (45), (48) and (50), we find that F_H is as in (51) with $h_0 = 0$, and that

$$F_x = \frac{6Q}{(H-\alpha)^2} - \frac{4}{\alpha}\log x^*, \tag{101}$$

$$F_y = -\frac{6Q}{H(H-\alpha)^2} + \frac{6}{\alpha^2}\log x^*, \tag{102}$$

$$F_0 = \frac{4}{\alpha}\log x^* + \frac{2\ell(3Q-2H)}{H^2}, \tag{103}$$

and

$$M = \frac{3}{\alpha^3}\left[\frac{Q(2H^2 - 3H\alpha + 2\alpha)\alpha}{H(H-\alpha)^2} + 2Q\log\frac{H-\alpha}{H} - \alpha(1-x^*) - 2\log x^*\right]. \tag{104}$$

These quantities are finite for $|p^*|$ finite, but are singular in the no-cavitation limit $p^* \to -\infty$ ($x^* \to 0^+$).

[2] Commonly in lubrication analyses with cavitation the relevant flux is unknown *a priori*, and an additional boundary condition (such as $\mathrm{d}p_1/\mathrm{d}x = 0$ at $x = x^*$) is imposed (see, for example, Szeri [23, p. 98]). In the present problem the flux is known ($Q_1 = 0$), and there is no freedom to impose such an additional boundary condition.

4. Three-dimensional flow

In a SSHE the process material not only undergoes flow in the transverse section (caused by the rotation of the rotor), but also is driven longitudinally along the annular gap between stator and rotor by an imposed axial pressure gradient (including, if the SSHE is mounted vertically, the effect of gravity).

To model this fully three-dimensional flow we consider briefly the effect of allowing flow along the channel in the z direction, in addition to the flow in the (x, y) plane, discussed above. We take the blades to be very long in the z direction, and suppose (quite realistically) that the dimensional axial length scale L_z satisfies $L_z \gg H$, so that the longitudinal flow can be assumed to be rectilinear.

We restrict attention to the case of steady flow of a Newtonian fluid satisfying the no-slip condition on all rigid boundaries. The analysis is valid whether or not the blade makes contact with the channel walls (though if there is contact with the moving wall then we assume for simplicity that cavitation does not occur).

Since the longitudinal flow is rectilinear, the flow in the z direction uncouples from that in the (x, y) plane. Thus with velocities and pressures denoted by $u_k\,\mathbf{i} + v_k\,\mathbf{j} + w_k\,\mathbf{k}$ and P_k for $k = 1, 2, 3$ (with u_k, v_k, w_k and P_k functions of x, y and z), we find straightforwardly that

$$w_1 = \frac{G}{2}y(h-y), \quad w_2 = \frac{G}{2}(H-y)(y-h), \quad w_3 = \frac{G}{2}y(H-y), \tag{105}$$

$$P_k = -Gz + p_k, \tag{106}$$

where $G = -\partial P_k/\partial z$ is the (constant) prescribed axial pressure gradient, and the velocity components $u_k = u_k(x, y)$ and $v_k = v_k(x, y)$ and the pressure contributions $p_k = p_k(x, y)$ are exactly as given for the two-dimensional transverse flow described in detail in section 2, so that all the results presented in section 2 go over to this three-dimensional case. Overall the fluid particles undergo a rather complicated fully three-dimensional motion down the channel; the earlier streamline plots, for example, are now to be interpreted as projections of the flow onto the transverse (x, y) plane.

The volume flux of fluid in the axial direction across the section $0 \le x \le 1+\ell$, $0 \le y \le H$ (non-dimensionalised with $GLh_{\rm p}^3/\mu$), namely

$$Q_z = \int_0^1 \int_0^h w_1 \,\mathrm{d}y\,\mathrm{d}x + \int_0^1 \int_h^H w_2 \,\mathrm{d}y\,\mathrm{d}x + \int_1^{1+\ell} \int_0^H w_3 \,\mathrm{d}y\,\mathrm{d}x, \tag{107}$$

is given by

$$Q_z = \frac{GH}{24}\left[2(h_0^2 + h_0h_1 + h_1^2) - 3H(h_0+h_1) + 2H^2(1+\ell)\right]. \tag{108}$$

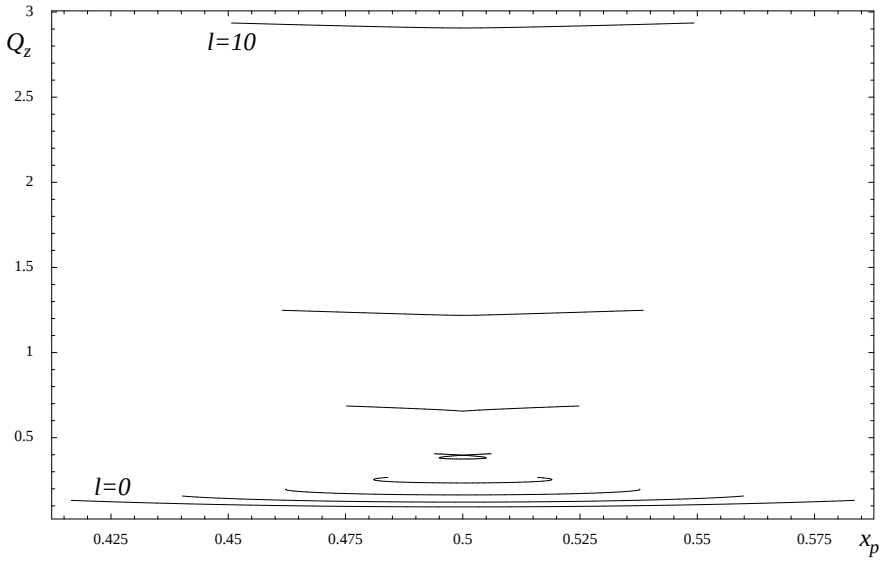

Figure 15. Plot of the axial volume flux Q_z given by (108) as a function of $x_{\rm p}$ in the case $H = \frac{3}{2}$, for $\ell = 0$, 0.1, 0.25, 0.5, 1, 2, 4, 10.

Figure 15 shows the axial flux Q_z plotted as a function of $x_{\rm p}$ for $H = \frac{3}{2}$ and various values of ℓ, in a case when the blade is not in contact with the channel walls. In particular, Figure 15 shows that Q_z varies relatively little with $x_{\rm p}$ in these cases.

In the case of blade contact at $x = 0$ (so that $h_0 = 0$ and $h_1 = \alpha$) the flux Q_z (for given values of G, H and ℓ) has a maximum value $GH^3(1+\ell)/12$ when $\alpha = 0$, a minimum value $GH^3(7+16\ell)/192$ when $\alpha = \frac{3}{4}H$, and takes the value $GH^3(1+2\ell)/24$ when $\alpha = H$.

The forces F_x, F_y, F_0 and F_H are exactly as given in (46), (47), (49) and (51). The force (per unit length in the axial direction) in the z direction on the blade due to the fluid (non-dimensionalised with $GLh_{\rm p}$) is given by

$$F_z = -\int_0^1 \left(\frac{\partial w_1}{\partial y} - \frac{\partial w_2}{\partial y}\right)_{y=h} {\rm d}x = \frac{GH}{2}, \tag{109}$$

and the forces (per unit length in the axial direction) in the z direction on the portions $0 \le x \le 1+\ell$ of the lower wall $y = 0$ and the upper wall $y = H$ due to the fluid (also non-dimensionalised with $GLh_{\rm p}$) are

$$\tilde{F}_0 = \int_0^1 \left.\frac{\partial w_1}{\partial y}\right|_{y=0} {\rm d}x + \int_1^{1+\ell} \left.\frac{\partial w_3}{\partial y}\right|_{y=0} {\rm d}x = \frac{G}{4}[2H\ell + h_0 + h_1] \tag{110}$$

and

$$\tilde{F}_H = -\int_0^1 \left.\frac{\partial w_2}{\partial y}\right|_{y=H} \mathrm{d}x - \int_1^{1+\ell} \left.\frac{\partial w_3}{\partial y}\right|_{y=H} \mathrm{d}x = \frac{G}{4}[2H(1+\ell) - h_0 - h_1], \tag{111}$$

respectively. As a check we note that the total force (per unit length in the axial direction) in the z direction acting on the fluid in $0 \le x \le 1+\ell$, $0 \le y \le H$, namely $GH(1+\ell) - F_z - \tilde{F}_0 - \tilde{F}_H$, is identically zero, as it should be. The dimensional power (per unit length in the axial direction) required to drive the axial flow is simply NGQ_z.

5. Conclusions

We have presented a simple mathematical model of fluid flow in a common type of SSHE in which the gaps between the blades and the device walls are narrow, so that a lubrication-theory description of the flow is valid. Specifically we analysed steady isothermal flow of a Newtonian fluid around a periodic array of pivoted scraper blades in a channel with one stationary and one moving wall, when there is an applied pressure gradient in a direction perpendicular to the wall motion. The flow is fully three-dimensional, but decomposes naturally into a two-dimensional "transverse" flow driven by the boundary motion and a "longitudinal" pressure-driven flow.

Firstly details of the structure of the transverse flow were considered. The analysis reveals that there is a range of blade-pivot positions $x_{\mathrm{p,min}} \le x_{\mathrm{p}} \le x_{\mathrm{p,max}}$ around $x_{\mathrm{p}} = \frac{1}{2}$ for which the desired contact between the blade tip and the scraped surface does not occur. Moreover, for such a value of x_{p} there can be as many as three different possible steady solutions each with different blade angles and flow patterns. The present calculations also reveal details of the flow structure, including the possible presence of regions of reversed flow under the blades. In addition predictions for the forces on the blades and the torque on the rotor, as well as the fluxes of fluid above and below the blades, were determined analytically.

It was shown that locating the pivot sufficiently near the end $x = 1$ (as is typically done in practice in SSHE design) will ensure that the blade tip at $x = 0$ will indeed make the desired contact with the scraped surface. However, the solution in this case predicts that the forces on the blades are singular and that an infinitely large torque is required to turn the rotor. These unrealistic predictions indicate that one or more effects neglected in the simple model become significant in this case. Three possible generalisations of the model (namely, allowing non-

Newtonian power-law fluid behaviour, including slip at the boundaries of region 1, and allowing for cavitation in regions of very low pressure) were shown to resolve these singularities.

Lastly the longitudinal flow was considered. Expressions were derived for the axial flux generated by a given pressure gradient, and for the associated axial forces on the blade and channel walls.

The simple model presented here adds to the quantitative understanding of some of the basic features of the fluid flow within a SSHE and provides a basis for subsequent studies of more complicated physical effects. In particular, the present results highlight the importance of positioning the pivot near the right-hand end of the blade, as well as providing relatively simple analytical expressions for the forces on the blades, rotor and stator and the torque on the blades which may help to inform the design process, and so help to produce improved designs with reduced blade wear and reduced power consumption.

In addition to non-isothermal effects, it would be useful to extend the analysis to investigate other practically important features neglected in this simple model, including blade wear, the effects of holes in the blades, and the possibility of unsteady flow.

Acknowledgements

This work forms part of a larger research project supported by the EPSRC (Research Grant GR/R993032, Principal Investigator Prof. C. P. Please, School of Mathematics, University of Southampton), and by Chemtech International and Tetra Pak, under the auspices of the Faraday Partnership for Industrial Mathematics, managed by the Smith Institute. In particular, thanks are due to Profs C. P. Please and A. D. Fitt, School of Mathematics, University of Southampton, Prof. D. L. Pyle and Dr K.-H. Sun, School of Food Biosciences, University of Reading, Dr N. Hall Taylor, Chemtech International Ltd, Reading, Dr J. Mathisson, Tetra Pak, and Dr H. Tewkesbury, Smith Institute, for many useful discussions.

Appendix

In this Appendix we state some of the lengthier equations relating to the problem of two-dimensional flow in a channel with a periodic array of blades, in the general case (discussed in section 2) when the blades are not in contact with the walls of the channel.

The Q_k ($k = 1, 2, 3$) obtained from (24) and (30)–(32) take the forms

$$Q_1 = \frac{h_0 h_1}{\Delta}\Big[H^3(2H - h_0 - h_1) + \ell\Big\{2(H - h_0)^2(H - h_1)^2 + H(2H - h_0 - h_1)h_0 h_1\Big\}\Big], \quad \text{(A1)}$$

$$Q_2 = \frac{\ell}{\Delta}(H - h_0)^2(H - h_1)^2\left[H(h_0 + h_1) - 2h_0 h_1\right], \quad \text{(A2)}$$

$$Q_3 = \frac{H}{\Delta}\Big[H^2(2H - h_0 - h_1)h_0 h_1 + \ell\Big\{(h_0 + h_1)(H - h_0)^2(H - h_1)^2 + (2H - h_0 - h_1)h_0^2 h_1^2\Big\}\Big], \quad \text{(A3)}$$

where

$$\Delta = H^3(2H - h_0 - h_1)(h_0 + h_1) + 2\ell\Big[(h_0 + h_1)(H - h_0)^2(H - h_1)^2 + (2H - h_0 - h_1)h_0^2 h_1^2\Big]. \quad \text{(A4)}$$

Then $p_0 - p_L$ may be obtained from (32).

The condition that the moment of forces (33) on the blade vanish can be written in several equivalent forms, including

$$\frac{2}{\alpha}\log\frac{h_1}{h_0} - \frac{\alpha + 2}{h_1} + \left[\frac{2}{\alpha}\log\frac{h_1}{h_0} - \frac{2\alpha + h_0(h_0 + h_1)}{h_0 h_1^2}\right]Q_1 + \left[\frac{2}{\alpha}\log\frac{H - h_1}{H - h_0} - \frac{2(H - 1)\alpha - (H - h_0)(2H - h_0 - h_1)}{(H - h_0)(H - h_1)^2}\right]Q_2 = 0. \quad \text{(A5)}$$

The algebraic transcendental equation (34) determining α as a function of x_p, H and ℓ, from which the results of section 2 were derived, is obtained by eliminating the Q_k from (A1)–(A5), and using (8).

References

1. M. Stranzinger, K. Feigl and E. Windhab, Non-Newtonian flow behaviour in narrow annular gap reactors. *Chem. Eng. Sci.* 56 (2001) 3347–3363.
2. A. D. Fitt and C. P. Please, Asymptotic analysis of the flow of shear-thinning foodstuffs in annular scraped heat exchangers. *J. Eng. Math.* 39 (2001) 345–366.
3. K.-H. Sun, D. L. Pyle, A. D. Fitt, C. P. Please, M. Baines and N. Hall-Taylor, Numerical study of 2D heat transfer in a scraped surface heat exchanger. *Computers and Fluids* 33 (2003) 869–880.
4. M. Härröd, Methods to distinguish between laminar and vortical flow in scraped surface heat exchangers. *J. Food Proc. Eng.* 13 (1990) 39–57.

5. W. Wang, J. H. Walton and K. L. McCarthy, Flow profiles of power law fluids in scraped surface heat exchanger geometry using MRI. *J. Food Proc. Eng.* 22 (1999) 11–27.
6. S. Rodruiguez, Flow measurements in scraped surface heat exchangers. PhD thesis, University of Birmingham, UK (2000).
7. M. Härröd, Scraped surface heat exchangers: a literature survey of flow patterns, mixing effects, residence time distribution, heat transfer and power requirements. *J. Food Proc. Eng.* 9 (1986) 1–62.
8. C. S. Rao and R. W. Hartel, Scraped surface heat exchangers. *Critical Reviews in Food Science and Nutrition* 46 (2006) 207–219.
9. Practical mathematical models for scraped surface heat exchangers. *Mathematics Today* 42 (2006) 124–125.
10. A. D. Fitt, M. E. M. Lee and C. P. Please, Analysis of heat flow and "channelling" in a scraped surface heat exchanger. To appear in *J. Eng. Math.* (2006).
11. C.-H. Ho and Y.-C. Tai, Micro-electro-mechanical systems (MEMS) and fluid flows. *Ann. Rev. Fluid Mech.* 30 (1998) 579–612.
12. V. Kaajakari and A. Lal, Thermokinetic actuation for batch assembly of microscale hinged structures. *J. Microelectromechanical Systems* 12 (2003) 425–432.
13. C. S. Peskin, The fluid dynamics of heart valves: experimental, theoretical, and computational methods. *Ann. Rev. Fluid Mech.* 14 (1982) 235–259.
14. W. R. Penney, Agitated vessels. In: G. F. Hewitt (ed.), *The Heat Exchanger Design Handbook.* New York: Begell House (2002) section 3.14.
15. A. A. Raimondi and J. Boyd, Applying bearing theory to the analysis and design of pad-type bearings. *Trans. ASME* 77 (1955) 287–309.
16. A. A. Raimondi and J. Boyd, The influence of surface profile on the load capacity of thrust bearings with centrally pivoted pads. *Trans. ASME* 77 (1955) 321–330.
17. W. J. Silliman and L. E. Scriven, Slip of liquid inside a channel exit. *Phys. Fluids* 21 (1978) 2115–2116.
18. D. E. Weidner and L. W. Schwartz, Contact-line motion of shear-thinning liquids. *Phys. Fluids* 6 (1994) 3535–3538.
19. M. W. Johnson and S. Mangkoesoebroto, Analysis of lubrication theory for the power law fluid. *Trans. ASME J. Tribol.* 115 (1993) 71–77.
20. A. B. Ross, S. K. Wilson and B. R. Duffy, Blade coating of a power-law fluid. *Phys. Fluids* 11 (1999) 958–970.
21. H. P. Greenspan, On the motion of a small viscous droplet that wets a surface. *J. Fluid Mech.* 84 (1978) 125–143.
22. L. M. Hocking, Sliding and spreading of thin two-dimensional drops. *Q. J. Mech. Appl. Math.* 34 (1981) 37–55.
23. A. Z. Szeri, *Fluid Film Lubrication: Theory and Design.* Cambridge (1998) 414pp.